https://doi.org/10.5194/egusphere-2025-2901
Preprint. Discussion started: 5 August 2025

Automatic reduction of ocean biogeochemical models: a case study with BFM (v5.3)

Malik J. Jordan[1], Emily F. Klee[1], Peter E. Hamlington[2], Nicole S. Lovenduski[3], and Kyle E. Niemeyer[1]

[1]School of Mechanical, Industrial, and Manufacturing Engineering, Oregon State University, Corvallis, OR, USA
[2]Paul M. Rady Department of Mechanical Engineering, University of Colorado, Boulder, CO, USA
[3]Department of Atmospheric and Oceanic Sciences, University of Colorado, Boulder, CO, USA

Correspondence: K. E. Niemeyer (kyle.niemeyer@oregonstate.edu)

Abstract. Modeling biogeochemical processes in ocean fluid dynamics simulations is computationally expensive, necessitating efficient model reduction techniques. Large-scale biophysical simulations, such as high-resolution large-eddy simulations (LES) of the upper ocean, require significant computing resources to capture small-scale turbulent processes while also resolving the evolution of reactive biogeochemical tracers. However, the complexity of existing biogeochemical models, such as the Biogeochemical Flux Model (BFM) which resolves 56 state variables, leads to unfeasibly high computational costs when represented in detailed LES. To address this, we applied model reduction techniques from the field of combustion to systematically reduce the complexity of the BFM while maintaining high fidelity. Specifically, we developed a modified version of the Directed Relation Graph with Error Propagation method and applied it to a 50-state-variable BFM. By analyzing 24 reduction scenarios, we produced five reduced models containing between 1 and 36 state variables capable of accurately capturing trends in concentration of the target fields. The results demonstrate the effectiveness of this reduction approach in preserving key biogeochemical dynamics while significantly reducing model size and complexity, paving the way for more efficient high-resolution ocean biogeochemical simulations.

https://doi.org/10.5194/egusphere-2025-2901
Preprint. Discussion started: 5 August 2025

1 Introduction

Ocean biogeochemical modeling has emerged as a key tool for investigating a wide range of biogeochemical processes in the ocean, with applications to studies of ocean carbon cycling, acidification, deoxygenation, and fisheries science (Fennel et al., 2022). Ocean biogeochemical models range in complexity from simple, nutrient-phytoplankton-zooplankton (NPZ) (Franks, 2002; Lewis, 2005) or nutrient-phytoplankton-zooplankton-detritus (NPZD) (Denman and Peña, 2002; Schartau and Oschlies, 2003; Heinle and Slawig, 2013) models that contain only three or four state variables, to complex NPZD-type models containing 20 or more state variables, such as the Biogeochemical Elemental Cycling (BEC) model (Moore et al., 2013); the Biogeochemical Flux Model (BFM) (Vichi et al., 2007b); the Carbon, Ocean, Biogeochemistry and Lower Trophics (COBALT) model (Stock et al., 2014, 2020); the Ecological Simulation (EcoSim) model (Bissett et al., 1999); and the biogeochemical MIRO model (Lancelot et al., 2005). Higher-complexity biogeochemical models contain multiple phytoplankton, zooplankton, and bacteria functional groups, and carry multiple limiting nutrients such as nitrate, ammonium, and iron.

Ocean biogeochemical models are coupled with physical circulation models to represent the physical transport and mixing of dissolved and suspended components critical for biogeochemical cycling. One-dimensional (depth) and three-dimensional (latitude, longitude, depth) models of physical circulation span a range of spatial resolutions (meters to hundreds of kilometers) and model domains (regional to global). Limited computational resources often require biogeochemical model complexity to be balanced by physical model complexity, for example, by simulating complex biogeochemical processes across the global ocean at coarse resolution (hundreds of kilometers) to represent processes important for global carbon cycling, or by simulating a simplified version of biogeochemical cycling in a small region at high resolution to capture the role of eddies or submesoscale processes on phytoplankton abundance.

Modeling the interactions between reactive ocean biogeochemical tracers and small-scale ocean circulation processes requires high levels of both physical and biogeochemical model complexity. This is because the mixing timescales of small-scale turbulence (1 m–1 km) are similar to the biogeochemical reaction timescales (Smith et al., 2015). Yet, past studies addressing physical–biogeochemical interactions on small scales have used either highly complex biogeochemical models and simplified physical models (Benzi and Nelson, 2009; Smith et al., 2020), or, alternatively, complex physical models and simplified biogeochemical models (Lévy et al., 2001; Le Quéré et al., 2005; Wiggert et al., 2006; Smith et al., 2015, 2018). Simulating coupled physical and biogeochemical processes with sufficient complexity at small scales (e.g., within large eddy simulation or LES) requires extensive computational resources that are often beyond the reach of most scientific projects. These computational costs can be reduced with ocean biogeochemical model reduction techniques, wherein the number of biogeochemical reactive tracers is reduced without affecting model fidelity.

Recent studies have successfully coupled reduced forms of complex ocean biogeochemical models to small-scale physical models. Ward et al. (2013) removed processes involving unconstrained parameters, with a focus on balancing generality and uncertainty (rather than computational cost). Galbraith et al. (2015) compared the full-detail 30-tracer TOPAZ model against manually reduced models with three and six tracers, finding that the reduced models could reasonably capture spatial patterns

https://doi.org/10.5194/egusphere-2025-2901
Preprint. Discussion started: 5 August 2025

of nutrients and oxygen, and carbon uptake; however, the reduced models produced significant differences in organic matter cycling. Smith et al. (2018) used computational singular perturbation to reduce a detailed eight-species ocean carbonate chemistry model for coupling with LES (2.5 m resolution); the model reduction permitted a multi-hour simulation of the coupled model and produced high spatiotemporal variability in dissolved inorganic carbon. More recently, Smith et al. (2020) developed a reduced-order biogeochemical model and coupled this to the one-dimensional Princeton Ocean Model (POM). They manually reduced the BFM from 56 to 17 state variables by using intuition to remove state variables believed to be unimportant to open-ocean ecosystem dynamics. While successful, their ocean biogeochemical model reduction process would be difficult to replicate in other models.

The present study outlines the development and implementation of a model reduction method, based on techniques used in the combustion field, to obtain reduced forms of ocean biogeochemical models. We apply the method to the open-ocean, 56-state-variable BFM v5.3 (Vichi et al., 2023). We then couple the reduced forms of the BFM to the one-dimensional Princeton Ocean Model (POM1D) and verify the result by comparing to the fully coupled BFM-POM1D (Vichi et al., 2007a). As we will demonstrate, our reduced models maintain high fidelity at lower computational cost. While our study focuses on reducing the BFM, the model reduction technique can be applied to any ocean biogeochemical model.

2 Methods

This section first describes the physical transport model used in this work, as well as the biogeochemical model used here for demonstration. Second, we describe the theory behind an existing reduction method: directed relation graph with error propagation (DRGEP). Next, the modified DRGEP method developed for this research is described. Then, we provide a description of automation software for the modified DRGEP method.

2.1 Princeton Ocean Model

POM was originally developed by Blumberg and Mellor (1987) and is an open-source software package written in Fortran. It is a free surface, hydrostatic, primitive equation ocean circulation model that employs a sigma coordinate system scaled by the depth of the water column for the vertical coordinate. The prognostic state variables include temperature, salinity, and turbulent kinetic energy fields, with modifications allowing for diagnostic simulations using climatological data for temperature and salinity profiles. Vertical mixing coefficients are computed using a second-order turbulence closure sub-model. Appendix B contains a brief description of the governing equations for the diagnostic mode of POM1D, which is used in this study. Blumberg and Mellor (1987) and Mellor (2003) fully describe the three-dimensional POM and the one-dimensional version (POM1D), respectively. We rewrote POM1D in Python (pyPOM1D) (Jordan et al., 2025a) for coupling with the Python version of the BFM (Jordan et al., 2025a) and reduction software (Klee, 2020a), described next.

https://doi.org/10.5194/egusphere-2025-2901
Preprint. Discussion started: 5 August 2025

2.2 BFM model

The BFM was originally developed by Vichi et al. (2007b, 2023) and is implemented in an open-source software package written in Fortran. For the purposes of this research, the dimensional BFM was rewritten in Python (Klee, 2020b; Jordan et al., 2025a). The full BFM v5.3 contains 56 state variables and includes the cycling of iron. For this work, we did not include iron cycling, resulting in a model containing 50 state variables. The state variables are categorized into three different chemical functional families (CFFs): living organic (LO), non-living organic (NO), and inorganic (IO). Figure 1 shows a schematic of the interactions between the CFFs. Vichi et al. (2007b) provide a full description of BFM.

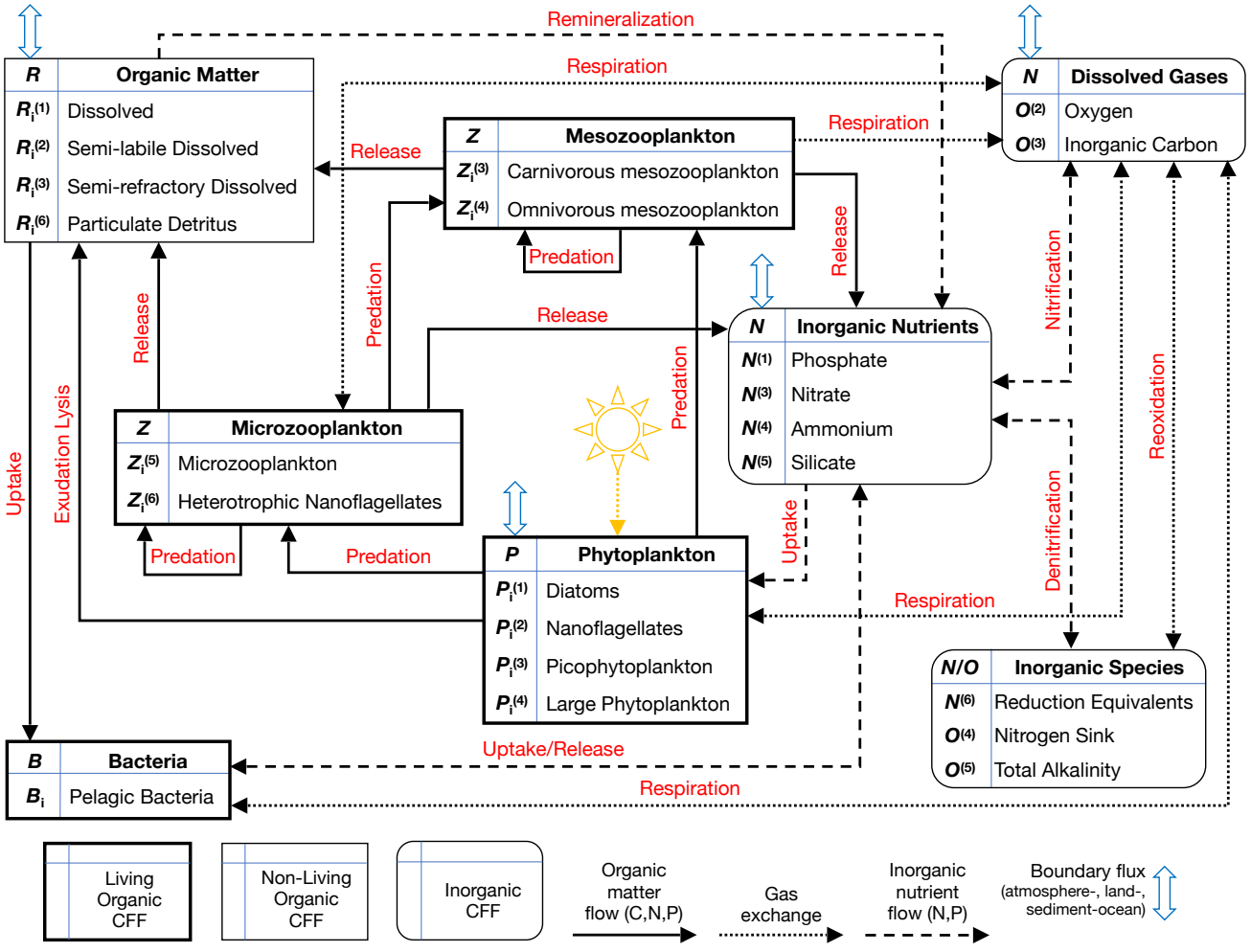

Figure 1. Schematic of the 50-state-variable BFM indicating the CFFs and the processes which transport matter; adapted from Vichi et al. (2007b).

https://doi.org/10.5194/egusphere-2025-2901
Preprint. Discussion started: 5 August 2025

2.3 DRGEP Method

In the field of combustion and gas-phase chemical kinetics, skeletal reduction methods are used to simplify complex chemical reaction models while preserving the essential kinetics and dynamics of the system. Skeletal reduction methods remove unimportant species and reactions for given conditions and applications to improve computational efficiency. DRGEP, like other skeletal reduction methods, is designed to be applied to chemical kinetic models in the form of a system of elementary chemical reactions. This is a limitation of these methods, because they can not easily be applied to models in the general form of ordinary differential equations (ODEs), like the BFM. This motivated the development of a modified DRGEP method that can reduce models not in the form of elementary reactions.

Pepiot-Desjardins and Pitsch (2008) first introduced the DRGEP method to improve on the original directed relation graph (DRG) method (Lu and Law, 2005, 2006a, b). This method represents a chemical kinetic model as a graph, as Figure 2 illustrates, where the nodes represent species and the weight and direction of the connecting lines represent the species dependencies, due to interactions in reactions. Species B and D are directly linked to the target species A and species C is directly linked to B. Removing species D introduces an estimated error of r_{AD} in the production rate of target A. Removing species C introduces an estimated error of r_{BC} to species B which propagates to A.

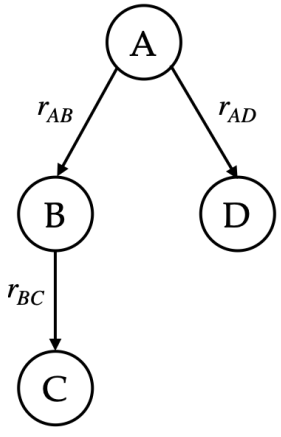

Figure 2. Example of a directed relation graph showing the direct interaction coefficients, r_{AB} , as the weight for the edge connecting each node/species.

Species dependencies are quantified using a direct interaction coefficient, which approximates the error induced in the net production of species A by the removal of species B from the model. The direct interaction coefficient is

$$r_{\mathrm{AB}} = \frac{\left|\sum_{i=1}^{n_R} \nu_{\mathrm{A},i}\omega_i\delta_{\mathrm{B}}^i\right|}{\max\left(P_{\mathrm{A}}, C_{\mathrm{A}}\right)}, \tag{1}$$

where

$$P_A = \sum_{i=1}^{n_R} \max\left(0, \nu_{A,i}\omega_i\right),$$

https://doi.org/10.5194/egusphere-2025-2901
Preprint. Discussion started: 5 August 2025

$$C_A = \sum_{i=1}^{n_R} \max\left(0, -\nu_{A,i}\omega_i\right),$$

$$\delta_{\mathrm{B}}^{i} = \begin{cases} 1, & \text{if the } i^{\text{th}} \text{ reaction involves species } B, \\ 0, & \text{otherwise,} \end{cases} \tag{2}$$

i is the i^{th} reaction, n_R is the total number of reactions, $\nu_{A,i}$ is the stoichiometric coefficient of species A in the i^{th} reaction, and ω_i is the overall reaction rate of the i^{th} reaction (Pepiot-Desjardins and Pitsch, 2008; Niemeyer et al., 2010; Niemeyer and Sung, 2011). Once the direct interaction coefficients are calculated, a modified version of Dijkstra's algorithm calculates the overall interaction coefficients (Dijkstra, 1959; Niemeyer and Sung, 2011):

$$R_{TB} = \max_{\text{all paths } p} \left(r_{TB,p}\right), \tag{3}$$

where the path-dependent interaction coefficient between target species T and species B along path p, $r_{TB,p}$, is

$$r_{TB,p} = \prod_{j=1}^{n-1} r_{S_j S_{j+1}}, \tag{4}$$

n is the number of species between T and B in pathway p, and S_j is a placeholder for the intermediate species j starting at T and ending at B.

After obtaining the overall interaction coefficient for each species, a user-defined cutoff threshold, ϵ, identifies species that can be removed. DRGEP removes any species and its associated reactions if the overall interaction coefficient for that species is less than the cutoff threshold. Previous research indicated that DRGEP offers improved reduction efficiency compared to DRG, in that it can remove more species for a given error tolerance (Pepiot and Pitsch, 2005; Pepiot-Desjardins and Pitsch, 2008; Niemeyer et al., 2010; Niemeyer and Sung, 2011).

2.4 Modified DRGEP

Next, we introduce the modified DRGEP method, which is similar to the DRGEP method but uses a modified direct interaction coefficient. The modification allows the method to be applied to a broader range of models, not just in the form of elementary chemical reactions, where nodes and edges are generalized to be any model component and interactions between them. Many biogeochemical models are in the form of ODEs and cannot be reduced using existing skeletal model reduction methods like DRGEP. The modified direct interaction coefficient was developed based on Pepiot-Desjardins and Pitsch (2008)'s original definition of the direct interaction coefficient: "r_{AB} quantifies how much removing B disturbs the established balance between production and consumption in the source term of A." The modified direct interaction coefficient is obtained by first generating the error matrix:

$$\begin{bmatrix} e_{C_1C_1} & \cdots & e_{C_1C_n} \\ \vdots & \ddots & \vdots \\ e_{C_nC_1} & \cdots & e_{C_nC_n} \end{bmatrix}, \tag{5}$$

https://doi.org/10.5194/egusphere-2025-2901
Preprint. Discussion started: 5 August 2025

where n is the number of species in the model, and the elements $e_{C_A C_B}$ are the percent error between the original rate of change in concentration for species A and the rate of change in concentration for species A after removing species B:

$$e_{C_A C_B} = \left| \frac{\frac{dC_A}{dt}\Big|^{\text{new}} - \frac{dC_A}{dt}\Big|^{\text{original}}}{\frac{dC_A}{dt}\Big|^{\text{original}}} \right| \cdot 100\% \,. \tag{6}$$

Next, the percent error matrix from Eq. (5) is normalized by the maximum value along each row in the matrix. This normalized matrix is the modified direct interaction coefficient matrix, where a given element would be calculated as

$$\tilde{r}_{C_A C_B} = \frac{e_{C_A C_B}}{\max(e_{C_A C_1}, e_{C_A C_2}, \ldots, e_{C_A C_n})} \,. \tag{7}$$

After calculating the modified direct interaction coefficients, the method follows the DRGEP method. Using the modified direct interaction coefficients, the overall interaction coefficients are calculated for a given target species as shown in Eqs. (3) and (4). Then, a user-defined cutoff threshold identifies which species can be removed. Any species whose overall interaction coefficient is less than the cutoff threshold can be removed.

2.5 Modified DRGEP Automation

The software developed for implementing the modified DRGEP method uses an automated reduction algorithm (Klee, 2020a). A specific scenario needs to be considered for the automation, because the algorithm iterates through different threshold values and checks the percent error introduced by the reduced model. This error is specific to a given scenario and is for quantities of interest to the user that are representative of a realistic use of the model. The iterations stop when the magnitude of the error exceeds a user-specified limit. The percent error between the full model and the reduced model determines the effectiveness of the reduced model being generated. This percent error can be characterized by the deviation from the full model for any combination of variables the user specifies. For example, it might be the percent error in the average concentration for a given species over a specified amount of time.

When using the automated reduction scenario, the following inputs are needed:

- The target species, which are the species of interest for the reduction scenario and overall interaction coefficients are calculated for each target species;
- Retained species, which are species that are also important and need to be kept in the reduced model, but do not affect the removal of any other species since overall interaction coefficients are not computed for them;
- The error function, which contains the calculation for the percent error being used in the reduction algorithm, and is specific for the scenario being considered;
- Error limit, which is a value the user determines, and is used to terminate the algorithm when the percent error exceeds this value;
- Function containing the rate equations for the model being reduced.

https://doi.org/10.5194/egusphere-2025-2901
Preprint. Discussion started: 5 August 2025

Once all of the inputs are provided, the program starts at a cutoff threshold, determines which species can be removed, removes them, then computes the error. If the error is less than the error limit, the program will increment the threshold value and repeat the reduction process. This loop is repeated until the error exceeds the specified error limit. The penultimate run conditions are used as the reduced model.

3 BFM Reduction

We configured the coupled pyPOM1D-BFM model to simulate seasonal phytoplankton dynamics within the upper 150 m of the ocean measured at the BATS location (Steinberg et al., 2001). Monthly climatologies of BATS were used as forcing data in the biophysical simulations assuming a 360-day climatological year with 12 months and 30 days per month. The modified DRGEP method was applied to the coupled pyPOM1D-BFM at multiple depths—air-sea interface (0 m), 25 m, 50 m, 75 m, 100 m, 125 m, and mixed layer bottom (150 m)—to consider surface, subsurface, and bottom effects while performing the model reduction analysis. Direct interaction coefficients were calculated for all state variables at each of the chosen depths. The maximum interaction coefficient was then selected for each state variable to ensure the reduced model obtained would be valid through the full domain. After the direct interaction coefficients and overall interaction coefficients are calculated, state variables are removed from the model based on the user-defined cutoff threshold.

To perform the model reduction we define a scenario that includes at least one target state variable and a specific percent error that controls the reduction. We chose the scenarios based on state variables typically of interest in the oceanic community, categorized into four sections: living organic (LO), dissolved inorganic carbon (DIC), particulate organic nitrogen (PON), inorganic nutrients (IN), and oxygen. The reduced model generated for each scenario is only valid for the conditions used for the reduction. We constructed a total of 24 different scenarios with relevant percent errors in either average concentration, peak concentration, or time of peak concentration for the given target state variables.

We forced the following state variables to be retained in all scenarios: ammonium ($N^{(4)}$) and all phytoplankton chlorophyll constituents ($P_{\text{chl}}^{(1)}$, $P_{\text{chl}}^{(2)}$, $P_{\text{chl}}^{(3)}$, $P_{\text{chl}}^{(4)}$). Nitrate ($N^{(3)}$) was also retained for the DIC4 scenario. We found that these state variables play important roles that are not completely captured using the interaction coefficients and need to be retained manually. This is consistent with prior applications of the DRGEP reduction method used in combustion, where inert species need to be protected from removal in the same way (Lu and Law, 2005, 2006a, b; Niemeyer et al., 2010).

3.1 Living Organic Scenarios

The LO CFF within the BFM includes four types of phytoplankton, pelagic bacteria, and four types of zooplankton. For the LO category, nine scenarios were considered, broken up into two sub-categories: phytoplankton chlorophyll and phytoplankton carbon. Six scenarios considered the phytoplankton chlorophyll concentrations and three considered phytoplankton carbon concentrations. The BFM contains four phytoplankton groups in the full BFM: diatoms ($P^{(1)}$), nanoflagellates ($P^{(2)}$), picophytoplankton ($P^{(3)}$), and large phytoplankton ($P^{(4)}$); and four zooplankton groups: carnivorous mesozooplankton ($Z^{(3)}$),

https://doi.org/10.5194/egusphere-2025-2901
Preprint. Discussion started: 5 August 2025

omnivorous mesozooplankton ($Z^{(4)}$), microzooplankton ($Z^{(5)}$), and heterotrophic nanoflagellates ($Z^{(6)}$). The scenarios, including the target state variables and the error being calculated for the reduction are:

LO1. This scenario measures the error in the average chlorophyll concentration (sum of $P_{\text{chl}}^{(1)}$, $P_{\text{chl}}^{(2)}$, $P_{\text{chl}}^{(3)}$, and $P_{\text{chl}}^{(4)}$) during the spring bloom, occurring January to March for the second year of a ten-year simulation.

LO2. This scenario is similar to Scenario 1 but excludes diatoms, and the error is in the average chlorophyll concentration (sum of $P_{\text{chl}}^{(2)}$, $P_{\text{chl}}^{(3)}$, and $P_{\text{chl}}^{(4)}$) during the spring bloom, occurring January to March for the second year of a ten-year simulation.

LO3. This scenario is similar to Scenario 2, but also excludes nanoflagellates and the error is in the average chlorophyll concentration (sum of $P_{\text{chl}}^{(3)}$ and $P_{\text{chl}}^{(4)}$) during the spring bloom occurring January to March for the second year of a ten-year simulation.

LO4. This scenario measures the error in the peak chlorophyll concentration (sum of $P_{\text{chl}}^{(1)}$, $P_{\text{chl}}^{(2)}$, $P_{\text{chl}}^{(3)}$, and $P_{\text{chl}}^{(4)}$) during the spring bloom occurring January to March for the second year of a ten-year simulation.

LO5. This scenario is similar to Scenario 4 but excludes diatoms, and the error is in the peak chlorophyll concentration (sum of $P_{\text{chl}}^{(2)}$, $P_{\text{chl}}^{(3)}$, and $P_{\text{chl}}^{(4)}$) during the spring bloom occurring January to March for the second year of a ten-year simulation.

LO6. This scenario is similar to Scenario 5 but also excludes nanoflagellates, and the error is in the peak chlorophyll concentration (sum of $P_{\text{chl}}^{(3)}$ and $P_{\text{chl}}^{(4)}$) during the spring bloom occurring January to March for the second year of a ten-year simulation.

LO7. This scenario looks at a spring phytoplankton bloom and measures the error in the average phytoplankton carbon concentration (sum of $P_{\text{C}}^{(1)}$, $P_{\text{C}}^{(2)}$, $P_{\text{C}}^{(3)}$, and $P_{\text{C}}^{(4)}$) during the spring bloom occurring January to March in the second year of a ten-year simulation.

LO8. This scenario looks at a spring phytoplankton bloom and measures the error in the peak phytoplankton carbon concentration (sum of $P_{\text{C}}^{(1)}$, $P_{\text{C}}^{(2)}$, $P_{\text{C}}^{(3)}$, and $P_{\text{C}}^{(4)}$) during the spring bloom occurring January to March in the second year of a ten-year simulation.

LO9. This scenario looks at a spring phytoplankton bloom and measures the error in the time at which the peak phytoplankton carbon concentration occurs (sum of $P_{\text{C}}^{(1)}$, $P_{\text{C}}^{(2)}$, $P_{\text{C}}^{(3)}$, and $P_{\text{C}}^{(4)}$) during the spring bloom occurring January to March in the second year of a ten-year simulation.

Eight of the Nine LO scenarios result in the same 34-state-variable model (BFM34) by removing the following state variables: silicate ($N^{(5)}$), reduction equivalents ($N^{(6)}$), diatom silicate ($P_{\text{S}}^{(1)}$), all mesozooplankton constituents ($Z_{\text{C}}^{(3)}$, $Z_{\text{N}}^{(3)}$, $Z_{\text{P}}^{(3)}$, $Z_{\text{C}}^{(4)}$, $Z_{\text{N}}^{(4)}$, $Z_{\text{P}}^{(4)}$), heterotrophic flagellates nitrogen $Z_{\text{N}}^{(6)}$, semi-labile dissolved organic carbon ($R_{\text{C}}^{(2)}$), semi-refractory dissolved organic carbon ($R_{\text{C}}^{(3)}$), particulate organic silicate ($R_{\text{S}}^{(6)}$), DIC ($O^{(3)}$), nitrogen sink ($O^{(4)}$), and total alkalinity ($O^{(5)}$). These state variables are not important when considering a phytoplankton spring bloom (for both carbon and chlorophyll concentra-

https://doi.org/10.5194/egusphere-2025-2901
Preprint. Discussion started: 5 August 2025

tions) and the amount of carbon stored in non-photosynthesizers. The one exception was scenario LO9, which removed the microzooplankton nitrogen constituent ($Z_{\mathrm{N}}^{(5)}$) and heterotrophic flagellates nitrogen ($Z_{\mathrm{N}}^{(6)}$) in addition to the 16 state variables listed above. We disregarded this 32-state-variable model because removing $Z_{\mathrm{N}}^{(5)}$ increases the error of the other LO scenarios beyond the error limit. Table 1 summarizes the reduction results for each scenario.

Table 1. Results from the model reduction for the LO scenarios showing which percent error is being calculated for the reduction, the target state variables, and the percent error for each scenario. The full BFM contains 50 state variables. The reduced model for LO1, LO2, LO3, LO4, LO5, LO6, LO7, and LO8 contains 34 state variables. The reduced model for LO9 contains 32 state variables.

Scenario	Error Description	Target State Variables	% Error	Error Units
LO1	Average	$P_{\mathrm{chl}}^{(1)}, P_{\mathrm{chl}}^{(2)}, P_{\mathrm{chl}}^{(3)}, P_{\mathrm{chl}}^{(4)}$	0.119	mg Chl-a m^{-3}
LO2	Average	$P_{\mathrm{chl}}^{(2)}, P_{\mathrm{chl}}^{(3)}, P_{\mathrm{chl}}^{(4)}$	0.400	mg Chl-a m^{-3}
LO3	Average	$P_{\mathrm{chl}}^{(3)}, P_{\mathrm{chl}}^{(4)}$	0.447	mg Chl-a m^{-3}
LO4	Peak	$P_{\mathrm{chl}}^{(1)}, P_{\mathrm{chl}}^{(2)}, P_{\mathrm{chl}}^{(3)}, P_{\mathrm{chl}}^{(4)}$	0.008	mg Chl-a m^{-3}
LO5	Peak	$P_{\mathrm{chl}}^{(2)}, P_{\mathrm{chl}}^{(3)}, P_{\mathrm{chl}}^{(4)}$	0.008	mg Chl-a m^{-3}
LO6	Peak	$P_{\mathrm{chl}}^{(3)}, P_{\mathrm{chl}}^{(4)}$	0.169	mg Chl-a m^{-3}
LO7	Average	$P_{\mathrm{C}}^{(1)}, P_{\mathrm{C}}^{(2)}, P_{\mathrm{C}}^{(3)}, P_{\mathrm{C}}^{(4)}$	0.138	mg C m^{-3}
LO8	Peak	$P_{\mathrm{C}}^{(1)}, P_{\mathrm{C}}^{(2)}, P_{\mathrm{C}}^{(3)}, P_{\mathrm{C}}^{(4)}$	0.032	mg C m^{-3}
LO9	Time of peak	$P_{\mathrm{C}}^{(1)}, P_{\mathrm{C}}^{(2)}, P_{\mathrm{C}}^{(3)}, P_{\mathrm{C}}^{(4)}$	1.350	mg C m^{-3}

3.2 Inorganic Nutrient Scenarios

The IN category considers four scenarios:

IN 1. This scenario measures the error in the average phosphate ($N^{(1)}$) concentration for the second year of a ten-year simulation.

IN 2. This scenario measures the error in the peak phosphate concentration during the second year of the ten-year simulation.

IN 3. This scenario measures the error in the average for the nitrate ($N^{(3)}$) concentration for the second year of a ten-year simulation.

IN 4. This scenario measures the error in the peak nitrate concentration that occurs during the second year of the ten-year simulation.

All four IN scenarios result in the same 34-state-variable model (BFM34) obtained in LO scenarios. Table 2 summarizes the reduction results for each IN scenario.

3.3 Particulate Organic Nitrogen Scenarios

The PON category considers three scenarios:

https://doi.org/10.5194/egusphere-2025-2901
Preprint. Discussion started: 5 August 2025

Table 2. Results from the model reduction for the inorganic nutrient scenarios showing which percent error is being calculated for the reduction, the target species, and the percent error for each scenario. The full BFM contains 50 state variables. The reduced model contains 34 state variables.

Scenario	Error Description	Target State Variables	% Error	Error Units
IN1	Average	$N^{(1)}$	0.201	mmol P_2 m^{-3}
IN2	Peak	$N^{(1)}$	0.101	mmol P_2 m^{-3}
IN3	Average	$N^{(3)}$	0.000	mmol N_2 m^{-3}
IN4	Peak	$N^{(3)}$	0.000	mmol N_2 m^{-3}

PON1. This scenario measures the error in a one-year average concentration for PON ($R_{\mathrm{N}}^{(6)}$) and phytoplankton nitrogen constituents ($P_{\mathrm{N}}^{(1)}$, $P_{\mathrm{N}}^{(2)}$, $P_{\mathrm{N}}^{(3)}$, $P_{\mathrm{N}}^{(4)}$) for the second year of a ten-year simulation.

PON2. This scenario measures the error in peak concentration for PON and phytoplankton nitrogen constituents during the second year of a ten-year simulation.

PON3. This scenario measures the error in the time at which the peak concentrations for PON and phytoplankton nitrogen constituents occur during the second year of a ten-year simulation.

PON1 and PON2 result in a 35-state-variable model (BFM35) removing: silicate ($N^{(5)}$), reduction equivalents ($N^{(6)}$), diatom silicate ($P_{\mathrm{S}}^{(1)}$), all mesozooplankton constituents ($Z_{\mathrm{C}}^{(3)}$, $Z_{\mathrm{N}}^{(3)}$, $Z_{\mathrm{P}}^{(3)}$, $Z_{\mathrm{C}}^{(4)}$, $Z_{\mathrm{N}}^{(4)}$, $Z_{\mathrm{P}}^{(4)}$), semi-labile dissolved organic carbon ($R_{\mathrm{C}}^{(2)}$), semi-refractory dissolved organic carbon ($R_{\mathrm{C}}^{(3)}$), particulate organic silicate ($R_{\mathrm{S}}^{(6)}$), DIC ($O^{(3)}$), nitrogen sink ($O^{(4)}$), and total alkalinity ($O^{(5)}$). PON3 resulted in the same 34-state-variable model produced in the LO scenarios. We disregarded this 34-state-variable model because removing $Z_{\mathrm{N}}^{(6)}$ increases the error of the other PON scenarios beyond the error limit.

Table 3. Results from the model reduction for the PON scenarios showing which percent error is being calculated for the reduction, the target state variables, and the percent error for each scenario. The full BFM contains 50 state variables. The reduced model for the PON scenarios contains 35 state variables.

Scenario	Error Description	Target State Variables	% Error	Error Units
PON1	Average	$P_{\mathrm{N}}^{(1)}$, $P_{\mathrm{N}}^{(2)}$, $P_{\mathrm{N}}^{(3)}$, $P_{\mathrm{N}}^{(4)}$, $R_{\mathrm{N}}^{(6)}$	0.105	mmol N m^{-3}
PON2	Peak	$P_{\mathrm{N}}^{(1)}$, $P_{\mathrm{N}}^{(2)}$, $P_{\mathrm{N}}^{(3)}$, $P_{\mathrm{N}}^{(4)}$, $R_{\mathrm{N}}^{(6)}$	0.036	mmol N m^{-3}
PON3	Time of peak	$P_{\mathrm{N}}^{(1)}$, $P_{\mathrm{N}}^{(2)}$, $P_{\mathrm{N}}^{(3)}$, $P_{\mathrm{N}}^{(4)}$, $R_{\mathrm{N}}^{(6)}$	4.890	mmol N m^{-3}

3.4 Oxygen Scenarios

The oxygen category considers four scenarios:

https://doi.org/10.5194/egusphere-2025-2901
Preprint. Discussion started: 5 August 2025

Oxygen1. This scenario measures the error in a one-month average for the oxygen ($O^{(2)}$) concentration in January of the second year of a ten-year simulation.

Oxygen2. This scenario measures the error in a one year average for the oxygen concentration in the second year of a ten-year simulation.

Oxygen3. This scenario measures the error in the peak oxygen concentration that occurs during the second year of the ten-year simulation.

Oxygen4. This scenario measures the error in the time at which the peak oxygen concentration occurs during the second year of the ten-year simulation.

The Oxygen1, Oxygen2, and Oxygen4 scenarios result in the same 35-state-variable (BFM35) model produced by the PON scenarios. Oxygen3 results in a six-state-variable model, which included oxygen and the five retained state variables. We then ran the scenario with the retained state variables removed to determine their impact of the peak oxygen concentration, resulting in a single-state-variable model with only oxygen. Table 4 summarizes the reduction results for each oxygen scenario.

Table 4. Results from the model reduction for the oxygen scenarios showing which percent error is being calculated for the reduction, the target state variable, and the percent error for each scenario. The full BFM contains 50 state variables. The reduced model for Oxygen1, Oxygen2, and Oxygen4 contains 35 state variables. The reduced model for Oxygen3 only includes oxygen.

Scenario	Error Description	Target State Variables	% Error	Error Units
Oxygen1	Average	$O^{(2)}$	0.082	mmol O_2 m^{-3}
Oxygen2	Average	$O^{(2)}$	0.108	mmol O_2 m^{-3}
Oxygen3	Peak	$O^{(2)}$	0.123	mmol O_2 m^{-3}
Oxygen4	Time of peak	$O^{(2)}$	0.000	mmol O_2 m^{-3}

The Oxygen3 scenario shows that all other state variables can be removed from the model without significantly impacting the peak oxygen concentration. This can be important in determining oxygen-minimum zones in the ocean—a fully detailed biogeochemical model is not necessary to model oxygen concentrations in the upper ocean. Though the rate equation for oxygen concentration depends on phytoplankton, bacteria, and zooplankton source/sink terms, peak oxygen concentration is driven more by the aeration at the ocean surface than the other source and sink terms. Oxygen aeration by wind depends on oxygen concentration and location-specific environmental parameters such as temperature, salinity, and wind speed. This suggests that this single-state-variable reduced model may only be valid for the parameters used in the BFM, and may not be suitable generally.

3.5 Dissolved Inorganic Carbon Scenarios

The DIC category considers four scenarios:

https://doi.org/10.5194/egusphere-2025-2901
Preprint. Discussion started: 5 August 2025

DIC1. This scenario measures the error in a one-month average for the DIC ($O^{(3)}$) concentration for January in the second year of a ten-year simulation.

DIC2. This scenario measures the error in a one-year average for the DIC concentration for the second year of a ten-year simulation.

DIC3. This scenario measures the error in a one year average for the DIC concentration for the fifth year of a ten-year simulation.

DIC4. This scenario measures the error in the peak DIC concentration that occurs during the second year of the ten-year simulation.

Three of the four DIC scenarios result in the same 36-state-variable model (BFM36) which removes silicate ($N^{(5)}$), reduction equivalents ($N^{(6)}$), diatom silicate ($P_{\mathrm{S}}^{(1)}$), all mesozooplankton constituents ($Z_{\mathrm{C}}^{(3)}$, $Z_{\mathrm{N}}^{(3)}$, $Z_{\mathrm{P}}^{(3)}$, $Z_{\mathrm{C}}^{(4)}$, $Z_{\mathrm{N}}^{(4)}$, $Z_{\mathrm{P}}^{(4)}$), semi-labile dissolved organic carbon ($R_{\mathrm{C}}^{(2)}$), semi-refractory dissolved organic carbon ($R_{\mathrm{C}}^{(3)}$), particulate organic silicate ($R_{\mathrm{S}}^{(6)}$), nitrogen sink ($O^{(4)}$), and total alkalinity ($O^{(5)}$). This model closely resembles BFM35, since DIC concentration is highly dependent on primary productivity.

The one exception was scenario DIC4, which results in a 23-state-variable model (BFM23) removing: silicate ($N^{(5)}$), reduction equivalents ($N^{(6)}$), all remaining diatom constituents ($P_{\mathrm{C}}^{(1)}$, $P_{\mathrm{N}}^{(1)}$, $P_{\mathrm{P}}^{(1)}$, $P_{\mathrm{S}}^{(1)}$), all remaining picophytoplankton constituents ($P_{\mathrm{C}}^{(3)}$, $P_{\mathrm{N}}^{(3)}$, $P_{\mathrm{P}}^{(3)}$), all remaining large phytoplankton constituents ($P_{\mathrm{C}}^{(4)}$, $P_{\mathrm{N}}^{(4)}$, $P_{\mathrm{P}}^{(4)}$), all mesozooplankton constituents ($Z_{\mathrm{C}}^{(3)}$, $Z_{\mathrm{N}}^{(3)}$, $Z_{\mathrm{P}}^{(3)}$, $Z_{\mathrm{C}}^{(4)}$, $Z_{\mathrm{N}}^{(4)}$, $Z_{\mathrm{P}}^{(4)}$), microzooplankton nitrogen ($Z_{\mathrm{N}}^{(5)}$), all heterotrophic flagellate constituents ($Z_{\mathrm{C}}^{(6)}$, $Z_{\mathrm{N}}^{(6)}$, $Z_{\mathrm{P}}^{(6)}$), semi-labile dissolved organic carbon ($R_{\mathrm{C}}^{(2)}$), semi-refractory dissolved organic carbon ($R_{\mathrm{C}}^{(3)}$), particulate organic silicate ($R_{\mathrm{S}}^{(6)}$), nitrogen sink ($O^{(4)}$), and total alkalinity ($O^{(5)}$). The DIC4 scenario originally produced a 22-state-variable model with nitrate ($N^{(3)}$) removed in addition to those removed in BFM23. Although nitrate's overall interaction coefficient designates it as an "unimportant" state variable for determining peak DIC concentration, it is necessary to retain all nutrients for biological processes when living organisms are present in a model. We therefore set nitrate as an additional retained state variable for the DIC4 scenario. The BFM23 reduced model is similar in size to the 17-state-variable model (BFM17) that Smith et al. (2020) produced manually. BFM23 includes bacteria, DIC, and three additional phytoplankton chlorophyll constituents not included in BFM17, while BFM17 includes the nitrogen constituent for microzooplankton not present in BFM23. Table 5 summarizes the reduction results for each DIC scenario.

4 Model Reduction Results

4.1 Physical Coupling to the Automatically Reduced BFM

We coupled each reduced model to the one-dimensional transport model, ran these to steady state, and calculated monthly means as functions of depth for chlorophyll-a, oxygen, nitrate, phosphate, PON, NPP, and DIC. We calculated normalized root mean squared error (NRMSE) to quantitatively evaluate the model. Root mean squared error (RMSE) was normalized by the

https://doi.org/10.5194/egusphere-2025-2901
Preprint. Discussion started: 5 August 2025

Table 5. Results from the model reduction for the DIC scenarios showing which percent error is being calculated for the reduction, the target state variable, and the percent error for each scenario. The full BFM contains 50 state variables. The reduced model for the DIC scenarios contains 36 state variables.

Scenario	Error Description	Target State Variable	% Error	Error Units
DIC1	Average, 1 month	$O^{(3)}$	0.124	mg C m^{-3}
DIC2	Average, year 2	$O^{(3)}$	0.106	mg C m^{-3}
DIC3	Average, year 5	$O^{(3)}$	0.117	mg C m^{-3}
DIC4	Peak, year 2	$O^{(3)}$	0.069	mg C m^{-3}

difference between the standard deviation in pyPOM1D-BFM50 for each concentration field.

$$\mathrm{RMSE} = \sqrt{\frac{\sum_{i=1}^{N} (x_i - y_i)^2}{N}} \tag{8}$$

$$\mathrm{NRMSE} = \frac{\mathrm{RMSE}}{\sigma} \times 100\%, \tag{9}$$

where N is the number of grid points in the concentration field and x_i and y_i are the concentrations at location i for the reduced and full models, respectively. The standard deviation in each field is

$$\sigma = \sqrt{\frac{\sum (x_i - \bar{x})^2}{N - 1}} \tag{10}$$

where $\bar{x}$ is the mean concentration in the field of interest.

Figures 3 and 4 show the NRMSEs in the fields of interest for each of the coupled physical-biogeochemical models. We find small RMSE values in the fields of interest in the 34-, 35-, and 36-state-variable models despite an approximate 30% reduction in size of the full model. A significant improvement in the representation of the Nitrate field can be seen between BFM34 and BFM35 with the inclusion of the heterotrophic flagellate nitrogen constituent ($Z_{\mathrm{N}}^{(6)}$. Large errors are observed in the targe fields for BFM17, which further demonstrates its loss of accuracy detailed by Smith et al. (2020). When compared to the manually reduced BFM17, the automatically reduced BFM23 provides a more accurate representation of the Oxygen, Phosphate, NPP, and DIC fields. With respect to the original, full model, the 1-, 23-, and 36-state-variable models were chosen as unique scenarios to be presented below. Due to similarities in size and performance to BFM36, we do not present the results for the less-detailed BFM34 and BFM35, but these can be found in Appendix C.

4.1.1 Single-Variable Oxygen Model

This oxygen model captures trends in the oxygen profile, including locations of maximum and minimum concentrations in the field. However, the oxygen concentration obtained from the reduced model is slightly lower than in the full model, particularly

https://doi.org/10.5194/egusphere-2025-2901
Preprint. Discussion started: 5 August 2025

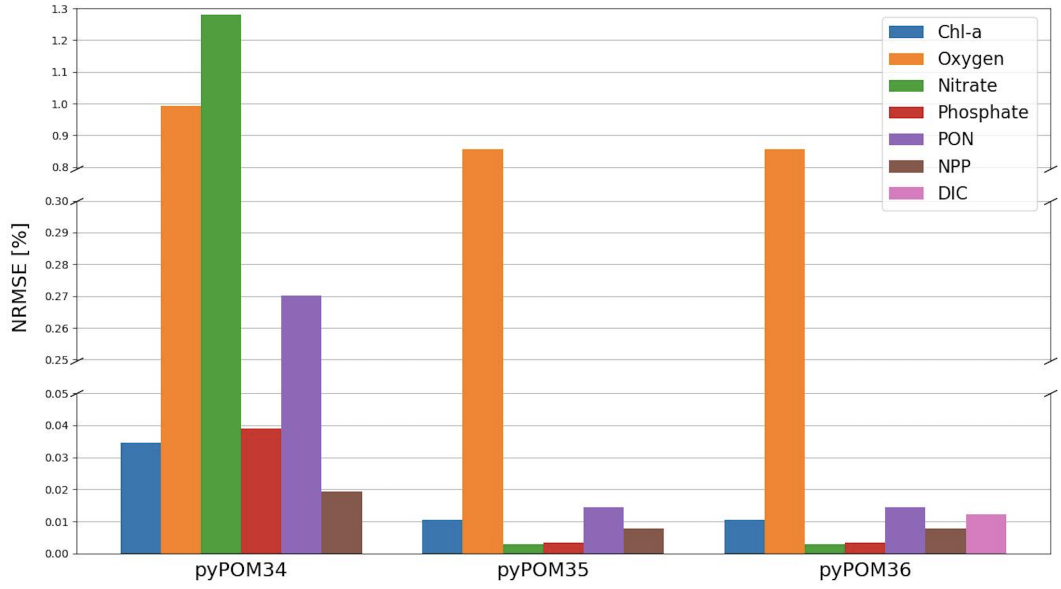

Figure 3. NRMSE (%) of the 34-, 35-, and 36-state variable models with respect to the full pyPOM1D-BFM50. Note the use of multiple y-axis limits to represent the error in the concentration fields on different scales. Error in DIC is not shown for BFM34 and BFM35 as the constituent is not resolved in the models.

in the subsurface region where primary production is the most prevalent. These results indicate the air-sea flux of oxygen is the primary driver of oxygen concentrations in the upper ocean. Figure 5 qualitatively compares the results to those obtained from the pyPOM1D-BFM50 in the second year of the simulation.

4.1.2 23-State-Variable BFM

Figure 6 qualitatively compares the results to those obtained from the pyPOM1D-BFM50. The 23-state-variable model successfully captures the trends in the profiles for each field of interest. In comparison to the full model, BFM23 produces oversaturated nitrate and phosphate fields and undersaturated PON and DIC fields. This comes from the removal of multiple living organisms in the model, resulting in lower nutrient consumption, respiration, and particulate nitrogen content. Chlorophyll-a and NPP concentrations are also undersaturated in the reduced model due to removing three of the four phytoplankton groups. Though the chlorophyll constituent of each phytoplankton group was retained during the reduction, chlorophyll synthesis highly depends on the carbon constituent (see Eq. A29). These results show the importance of parameter optimization following a model reduction, which is also evident in the manually reduced BFM17 (Smith et al., 2020). Kern et al. (2023) optimized BFM17 by performing an optimization-based parameter estimation of the 51 uncertain model parameters, finding improvement in total normalized error between 31% and 95% for five target fields—chlorophyll-a, oxygen, nitrate, phosphate, and PON. Appendix C provides a qualitative comparison of BFM23 to the manually reduced BFM17.

https://doi.org/10.5194/egusphere-2025-2901
Preprint. Discussion started: 5 August 2025

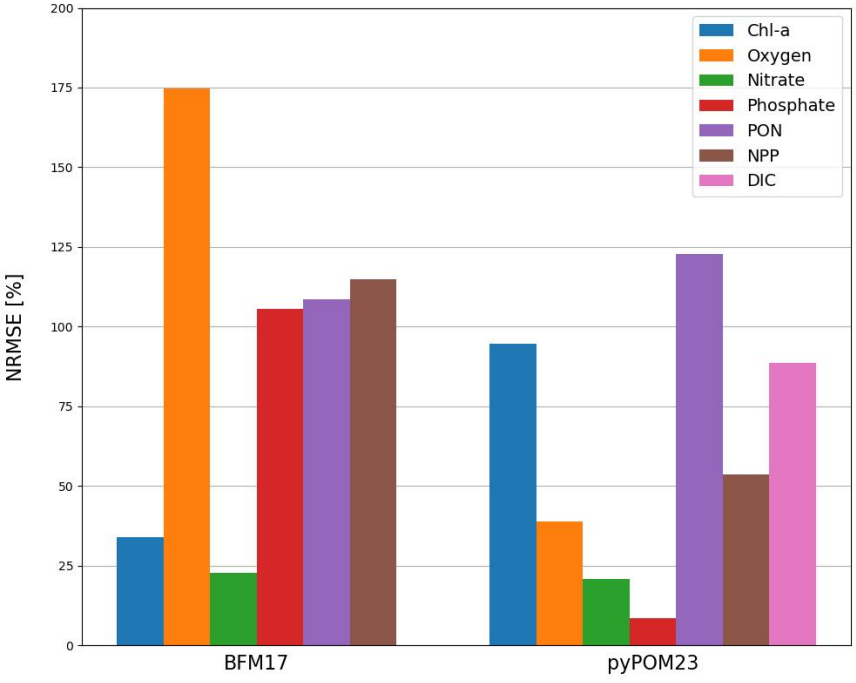

Figure 4. NRMSE (%) of the Fortran BFM17 with respect to BFM50 and Python BFM23 with respect to the full pyPOM1D-BFM50. Error in DIC is not shown for BFM17 as the constituent is not resolved in the model.

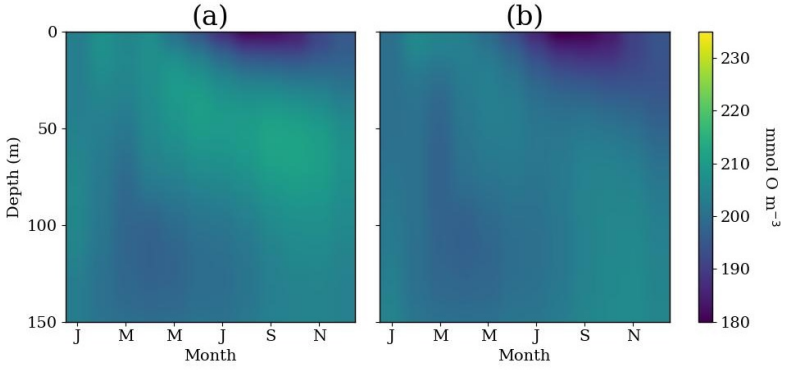

Figure 5. Comparison of (a) pyPOM1D-BFM50 simulation results to (b) pyPOM1D-Oxygen for oxygen concentration (mmol O/m^3).

https://doi.org/10.5194/egusphere-2025-2901
Preprint. Discussion started: 5 August 2025

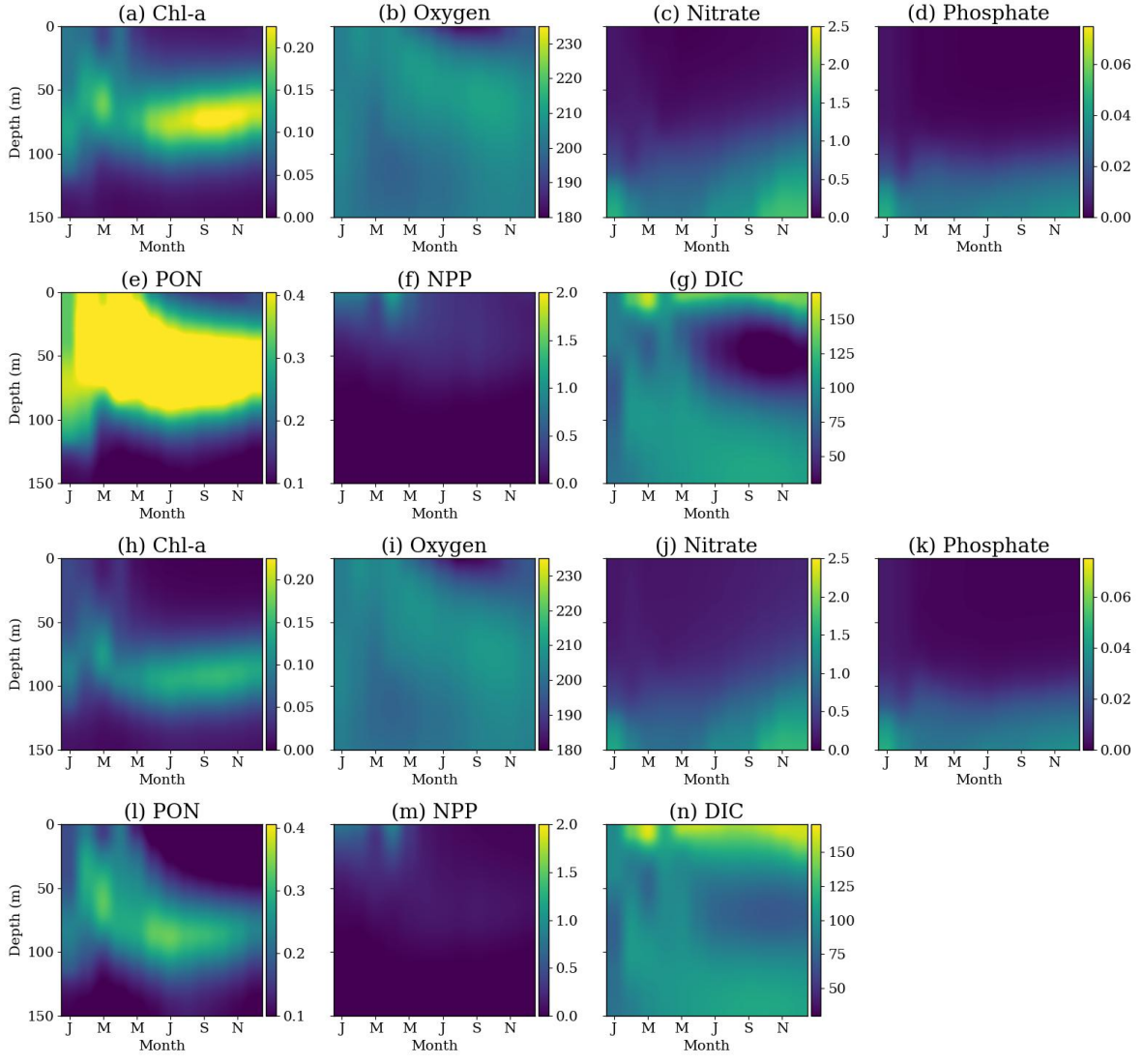

Figure 6. Comparison of pyPOM1D-BFM50 simulation results (rows 1 and 2) to pyPOM1D-BFM23 (rows 3 and 4) for (a,h) chlorophyll-a (mg Chl-a/m^3), (b,i) oxygen (mmol O/m^3), (c,j) nitrate (mmol N/m^3), (d,k) phosphate (mmol P/m^3), (e,l) PON (mg N/m^3), (f,m) NPP (mg C/m^3/day), (g,n) DIC (mg C/m^3).

https://doi.org/10.5194/egusphere-2025-2901
Preprint. Discussion started: 5 August 2025

4.1.3 36-State-Variable BFM

Figure 7 qualitatively compares the results of BFM36 to those obtained from pyPOM1D-BFM50. The 36-state-variable model provides the most accurate representation of the full BFM50, producing an NRMSE below 0.015% for all fields of interest apart from oxygen at 0.857%. This demonstrates the ability of the modified DRGEP method to identify and remove unnecessary state variables from complex biogeochemical models. The method determined the 14 state variables removed from BFM50 to produce BFM36 were determined to be unnecessary in all reduction scenarios.

4.1.4 Summary

Using a variety of scenarios, we reduced the 50-state-variable BFM to 1-, 23-, 34-, 35-, and 36-state-variable models. Ammonium ($N^{(4)}$) and all phytoplankton chlorophyll constituents ($P^{(1)}_{\text{chl}}$, $P^{(2)}_{\text{chl}}$, $P^{(3)}_{\text{chl}}$, $P^{(4)}_{\text{chl}}$) are retained in each scenario except Oxygen3, which produced the single-variable model. The following state variables are identified as unimportant across all scenarios: silicate ($N^{(5)}$), reduction equivalents ($N^{(6)}$), diatom silicate ($P^{(1)}_{\text{S}}$), all mesozooplankton constituents ($Z^{(3)}_{\text{C}}$, $Z^{(3)}_{\text{N}}$, $Z^{(3)}_{\text{P}}$, $Z^{(4)}_{\text{C}}$, $Z^{(4)}_{\text{N}}$, $Z^{(4)}_{\text{P}}$), semi-labile dissolved organic carbon ($R^{(2)}_{\text{C}}$), semi-refractory dissolved organic carbon ($R^{(3)}_{\text{C}}$), particulate organic silicate ($R^{(6)}_{\text{S}}$), nitrogen sink ($O^{(4)}$), and total alkalinity ($O^{(5)}$). Though these components could be removed from the BFM, we do not suggest that these components are universally unimportant. Rather, the reduced models obtained in this work apply only to the BFM for specific environmental conditions and tracer interactions. Changing such conditions requires the reduction strategies to be reapplied to a obtain reduced model that accurately represents the new system.

5 Conclusions

This study demonstrates a method for automatically reducing ocean biogeochemical models by adapting a technique used in the field of combustion: the DRGEP method. DRGEP identifies unimportant species and reactions that can be removed from the system without inducing substantial error. However, DRGEP is designed to be applied to chemical kinetic models in the form of elementary chemical reactions and cannot be easily applied to biogeochemical models in the form of ODEs. Here, we introduce the modified DRGEP method, suitable for a broader range of model types, to apply to biogeochemical models.

We apply the modified DRGEP method to the 50-state-variable BFM, considering 24 reduction scenarios in terms of different target state variables and/or types of error considered. The 24 scenarios are grouped into four categories: living organic, DIC, PON, and oxygen. These categories result in reduced models containing 1, 23, 34, 35, and 36 state variables. All reduction scenarios consistently eliminate 14 state variables: silicate ($N^{(5)}$), reduction equivalents ($N^{(6)}$), diatom silicate ($P^{(1)}_{\text{S}}$), all mesozooplankton constituents ($Z^{(3)}_{\text{C}}$, $Z^{(3)}_{\text{N}}$, $Z^{(3)}_{\text{P}}$, $Z^{(4)}_{\text{C}}$, $Z^{(4)}_{\text{N}}$, $Z^{(4)}_{\text{P}}$), semi-labile dissolved organic carbon ($R^{(2)}_{\text{C}}$), semi-refractory dissolved organic carbon ($R^{(3)}_{\text{C}}$), particulate organic silicate ($R^{(6)}_{\text{S}}$), nitrogen sink ($O^{(4)}$), and total alkalinity ($O^{(5)}$). We find that the reduction strategies are insensitive to the target state variables, which can be attributed to the strongly-coupled interactions between biogeochemical tracers.

https://doi.org/10.5194/egusphere-2025-2901
Preprint. Discussion started: 5 August 2025

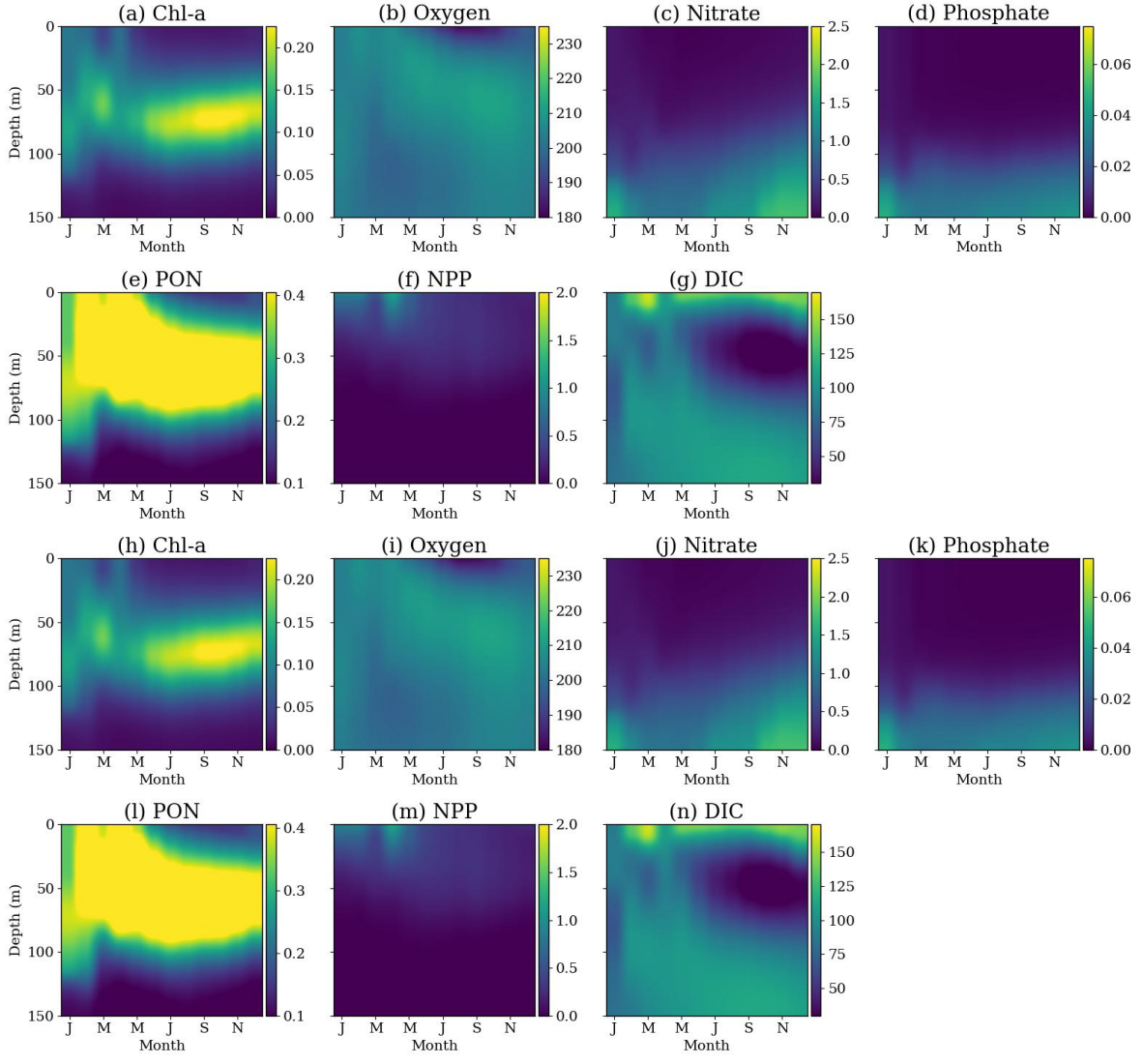

Figure 7. Comparison of pyPOM1D-BFM50 simulation results (rows 1 and 2) to pyPOM1D-BFM36 (rows 3 and 4) for (a,h) chlorophyll-a (mg Chl-a/m^3), (b,i) oxygen (mmol O/m^3), (c,j) nitrate (mmol N/m^3), (d,k) phosphate (mmol P/m^3), (e,l) PON (mg N/m^3), (f,m) NPP (mg C/m^3/day), (g,n) DIC (mg C/m^3).

https://doi.org/10.5194/egusphere-2025-2901
Preprint. Discussion started: 5 August 2025

We couple the reduced ocean biogeochemical models to a one-dimensional physical ocean model to examine the effect of vertical transport on tracer distributions. We compare results from the reduced models with the full 50-state-variable BFM for seven target fields of interest: chorophyll-a, oxygen, nitrate, phosphate, PON, NPP, and DIC. We find that the reduced models produce results comparable to the full BFM for the target state variables of the chosen reduction strategy, which demonstrates the effectiveness of the modified DRGEP method. Additionally, the modified DRGEP method produces a reduced model that is comparable in size to the manually reduced BFM17 with better performance, illustrating the utility of the method for inexperienced users of ocean biogeochemical models.

Future work should apply the automatic model reduction strategy to other ocean biogeochemical models. Additionally, the modified DRGEP method should be applied to the BFM using different observational data for environmental forcing to compare outputs for the reduction scenarios. It would be useful to perform a sensitivity analysis to identify and optimize the most sensitive model parameters for a more accurate representation of observational data. The current structure of the modified DRGEP method was designed for application to the BFM and cannot be directly applied to other biogeochemical models. This motivates the development of a generalized framework for ocean biogeochemical models capable of accurately representing models of varying structure and complexity to enable further implementation of the model reduction strategy.

Code and data availability. The current version of pyPOM1D-BFM is available from the project website https://github.com/MalikJordan/pyPOM1D-BFM under the BSD 3-clause license. The exact version of the model used to produce the results used in this paper is archived on Zenodo (Jordan et al., 2025a), as are input data and scripts to run the model and produce the plots for all the simulations presented in this paper (Jordan et al., 2025b).

https://doi.org/10.5194/egusphere-2025-2901
Preprint. Discussion started: 5 August 2025

A BFM Equations

The BFM is adapted from the original 56-state-variable model from Vichi et al. (2007b) (Vichi et al., 2023). We did not include iron cycling for this work, which resulted in a full model containing 50 state variables. A list of the state variables is provided in Table A1. The rate of change equations for each state variable are composed of source and sink terms from various physiological and ecological processes listed in Table A2 and are detailed below.

Table A1. List of the 50 state variables in the BFM, including the chemical functional family (CFF), units, description, and rate equation reference for each state variable. CFFs are divided into living organic (LO), non-living organic (NO), and inorganic (IO) families.

Symbol	CFF	Units	Description	Equation
$P_C^{(1)}$	LO	mg C m^{-3}	Diatoms Carbon	A4
$P_N^{(1)}$	LO	mmol N m^{-3}	Diatoms Nitrogen	A5
$P_P^{(1)}$	LO	mmol P m^{-3}	Diatoms Phosphorus	A6
$P_{chl}^{(1)}$	LO	mg Chl-a m^{-3}	Diatoms Chlorophyll	A7
$P_S^{(1)}$	LO	mmol Si m^{-3}	Diatoms Silicate	A8
$P_C^{(2)}$	LO	mg C m^{-3}	Nanoflagellates Carbon	A4
$P_N^{(2)}$	LO	mmol N m^{-3}	Nanoflagellates Nitrogen	A5
$P_P^{(2)}$	LO	mmol P m^{-3}	Nanoflagellates Phosphorus	A6
$P_{chl}^{(2)}$	LO	mg Chl-a m^{-3}	Nanoflagellates Chlorophyll	A7
$P_C^{(3)}$	LO	mg C m^{-3}	Picophytoplankton Carbon	A4
$P_N^{(3)}$	LO	mmol N m^{-3}	Picophytoplankton Nitrogen	A5
$P_P^{(3)}$	LO	mmol P m^{-3}	Picophytoplankton Phosphorus	A6
$P_{chl}^{(3)}$	LO	mg Chl-a m^{-3}	Picophytoplankton Chlorophyll	A7
$P_C^{(4)}$	LO	mg C m^{-3}	Large Phytoplankton Carbon	A4
$P_N^{(4)}$	LO	mmol N m^{-3}	Large Phytoplankton Nitrogen	A5
$P_P^{(4)}$	LO	mmol P m^{-3}	Large Phytoplankton Phosphorus	A6
$P_{chl}^{(4)}$	LO	mg Chl-a m^{-3}	Large Phytoplankton Chlorophyll	A7
B_C	LO	mg C m^{-3}	Pelagic Bacteria Carbon	A33
B_N	LO	mmol N m^{-3}	Pelagic Bacteria Nitrogen	A34
B_P	LO	mmol P m^{-3}	Pelagic Bacteria Phosphorus	A35

Continued on next page

https://doi.org/10.5194/egusphere-2025-2901
Preprint. Discussion started: 5 August 2025

Table A1 - Continued from previous page

Symbol	CFF	Units	Description	Equation
$Z_C^{(3)}$	LO	mg C m^{-3}	Carnivorous Mesozooplankton Carbon	A51
$Z_N^{(3)}$	LO	mmol N m^{-3}	Carnivorous Mesozooplankton Nitrogen	A52
$Z_P^{(3)}$	LO	mmol P m^{-3}	Carnivorous Mesozooplankton Phosphorus	A53
$Z_C^{(4)}$	LO	mg C m^{-3}	Omnivorous Mesozooplankton Carbon	A51
$Z_N^{(4)}$	LO	mmol N m^{-3}	Omnivorous Mesozooplankton Nitrogen	A52
$Z_P^{(4)}$	LO	mmol P m^{-3}	Omnivorous Mesozooplankton Phosphorus	A53
$Z_C^{(5)}$	LO	mg C m^{-3}	Microzooplankton Carbon	A51
$Z_N^{(5)}$	LO	mmol N m^{-3}	Microzooplankton Nitrogen	A52
$Z_P^{(5)}$	LO	mmol P m^{-3}	Microzooplankton Phosphorus	A53
$Z_C^{(6)}$	LO	mg C m^{-3}	Heterotrophic Nanoflagellates Carbon	A51
$Z_N^{(6)}$	LO	mmol N m^{-3}	Heterotrophic Nanoflagellates Nitrogen	A52
$Z_P^{(6)}$	LO	mmol P m^{-3}	Heterotrophic Nanoflagellates Phosphorus	A53
$R_C^{(1)}$	NO	mg C m^{-3}	Dissolved Organic Carbon	A74
$R_N^{(1)}$	NO	mmol N m^{-3}	Dissolved Organic Nitrogen	A75
$R_P^{(1)}$	NO	mmol P m^{-3}	Dissolved Organic Phosphorus	A76
$R_C^{(2)}$	NO	mg C m^{-3}	Semi-Labile Dissolved Organic Carbon	A77
$R_C^{(3)}$	NO	mg C m^{-3}	Semi-Refractory Dissolved Organic Carbon	A78
$R_C^{(6)}$	NO	mg C m^{-3}	Particulate Organic Carbon	A79
$R_N^{(6)}$	NO	mmol N m^{-3}	Particulate Organic Nitrogen	A80
$R_P^{(6)}$	NO	mmol P m^{-3}	Particulate Organic Phosphorus	A81
$R_S^{(6)}$	NO	mmol Si m^{-3}	Particulate Organic Silicate	A82
$N^{(1)}$	IO	mmol P m^{-3}	Phosphate	A88
$N^{(3)}$	IO	mmol N m^{-3}	Nitrate	A89
$N^{(4)}$	IO	mmol N m^{-3}	Ammonium	A90
$N^{(5)}$	IO	mmol Si m^{-3}	Silicate	A91
$N^{(6)}$	IO	mmol S m^{-3}	Reduction Equivalents	A95
$O^{(2)}$	IO	mmol O_2 m^{-3}	Dissolved Oxygen	A84
$O^{(3)}$	IO	mg C m^{-3}	Dissolved Inorganic Carbon	A85
$O^{(4)}$	IO	mmol N m^{-3}	Nitrogen Sink	A92
$O^{(5)}$	IO	mmol Eq m^{-3}	Total Alkalinity	A94

https://doi.org/10.5194/egusphere-2025-2901
Preprint. Discussion started: 5 August 2025

Table A2. List of abbreviations used to indicate physiological and ecological processes in the BFM equations.

Abbreviation	Process
gpp	Gross primary production
rsp	Respiration
prd	Predation
rel	Biological release: egestion, excretion, mortality
exu	Exudation
upt	Uptake
lys	Lysis
syn	Biochemical synthesis
nit	Nitrification
denit	Denitrification
rmn	Biochemical remineralization
reox	Reoxidation

Table A3. Symbols, values, units, and descriptions for constant parameters within the BFM.

Symbol	Value	Units	Description
$\Omega_{\mathrm{C}}^{(O)}$	12.0	mmol O_2 (mg C)$^{-1}$	Stiochiometric coefficient for oxygen reaction
$\Omega_{\mathrm{N}}^{(O)}$	2.0	mmol O_2 (mmol N)$^{-1}$	Stiochiometric coefficient for nitrification reaction
$\tilde{\Omega}_{\mathrm{N}}^{(O)}$	1.25	mmol O_2 (mmol N)$^{-1}$	Stiochiometric coefficient for denitrification reaction
$\Omega_{O}^{(r)}$	0.5	mmol HS^- (mmol O_2)$^{-1}$	Stiochiometric coefficient for oxic-anoxic reaction
$\Omega_{\mathrm{N}}^{(r)}$	0.625	mmol HS^- (mmol N)$^{-1}$	Stiochiometric coefficient for nitrogen-anoxic reaction
ε_{C}	0.6	-	Partition between dissolved and particulate excretion of carbon
ε_{N}	0.72	-	Partition between dissolved and particulate excretion of nitrogen
ε_{P}	0.832	-	Partition between dissolved and particulate excretion of phosphorus

https://doi.org/10.5194/egusphere-2025-2901
Preprint. Discussion started: 5 August 2025

A1 Environmental Parameters

The BFM depends on the following environmental parameters: temperature, surface irradiance, salinity, and wind speed. These parameters change seasonally and their values are calculated using a sinusoidal forcing based on summer and winter values. The effects of temperature on the physiological processes is denoted by a non-dimensional parameter $f_j^{(T)}$ defined as

$$f_j^{(T)} = Q_{10,j}^{(T-T^*)/T^*}, \quad j = P, Z, B, N, S \tag{A1}$$

where T^* is a base temperature and $Q_{10,j}$ is a a coefficient for phytoplankton ($j = P$), zooplankton ($j = Z$), bacterioplankton ($j = B$), nitrification/denitrification reaction ($j = N$), and the dissolution of biogenic silica ($j = S$). Irradiance directly affects phytoplankton growth during photosynthesis. The amount of photosynthetically available radiation (PAR) within the BFM is calculated as

$$E_{\text{PAR}} = \frac{Q_S\, \varepsilon_{\text{PAR}}}{0.217 \lambda \Delta z}(1 - \exp(-\lambda \Delta z)) \tag{A2}$$

where Q_S is the short-wave surface irradiance flux, ε_{PAR} is the fraction of PAR within Q_S, 0.217 is a conversion factor used to convert Q_S from units of $W\ m^{-2}$ to $\mu\ E\ m^{-2}\ s^{-1}$, λ is the total extinction coefficient, and Δz is the depth of the surface layer. The total extinction coefficient is calculated as

$$\lambda = \lambda_w + c_{R^{(6)}} R_{\text{C}}^{(6)} + \sum_{i=1}^{4} i P_{chl}^{(i)} \tag{A3}$$

where λ_w is the background extinction coefficient, $c_{R^{(6)}}$ if the specific attenuation coefficient of particulate detritus, and $P_{chl}^{(i)}$ are the phytoplankton chlorophyll terms for $i = 1, 2, 3, 4$.

A2 Living Organic Components

The living organic components include phytoplankton, bacteria, and zooplankton.

A2.1 Phytoplankton

Phytoplankton are a part of the living organic CFF and the BFM contains four phytoplankton species: diatoms, nanoflagellates, picophytoplankton, and large phytoplankton. Each phytoplankton species has carbon, nitrogen, phosphorous, chlorophyll, and silicate constituents, each representing a different state variable. The rate equations for each phytoplankton constituent are

$$\left.\frac{\partial P_{\text{C}}^{(i)}}{\partial t}\right|_{\text{bio}} = \left.\frac{\partial P_{\text{C}}^{(i)}}{\partial t}\right|_{O^{(3)}}^{\text{gpp}} - \left.\frac{\partial P_{\text{C}}^{(i)}}{\partial t}\right|_{O^{(3)}}^{\text{rsp}} - \sum_{j=1,6} \left.\frac{\partial P_{\text{C}}^{(i)}}{\partial t}\right|_{R_{\text{C}}^{(j)}}^{\text{lys}} - \left.\frac{\partial P_{\text{C}}^{(i)}}{\partial t}\right|_{R_{\text{C}}^{(2)}}^{\text{exu}} - \sum_{k=3}^{6} \left.\frac{\partial Z_{\text{C}}^{(k)}}{\partial t}\right|_{P_{\text{C}}^{(i)}}^{\text{prd}} \tag{A4}$$

$$\left.\frac{\partial P_{\text{N}}^{(i)}}{\partial t}\right|_{\text{bio}} = \max\left[0, \left.\frac{\partial P_{\text{N}}^{(i)}}{\partial t}\right|_{N^{(3)}}^{\text{upt}} + \left.\frac{\partial P_{\text{N}}^{(i)}}{\partial t}\right|_{N^{(4)}}^{\text{upt}}\right] - \sum_{j=1,6} \left.\frac{\partial P_{\text{N}}^{(i)}}{\partial t}\right|_{R_{\text{N}}^{(j)}}^{\text{lys}} - \frac{\partial P_{\text{N}}^{(i)}}{\partial P_{\text{C}}^{(i)}} \sum_{k=3}^{6} \left.\frac{\partial Z_{\text{C}}^{(k)}}{\partial t}\right|_{P_{\text{C}}^{(i)}}^{\text{prd}} \tag{A5}$$

https://doi.org/10.5194/egusphere-2025-2901
Preprint. Discussion started: 5 August 2025

Table A4. Symbols, values, units, and descriptions for environmental parameters within the BFM.

Symbol	Value	Units	Description
$Q_{10,P}$	2.0	-	Q_{10} coefficient for phytoplankton
$Q_{10,Z}$	2.0	-	Q_{10} coefficient for zooplankton
$Q_{10,B}$	2.95	-	Q_{10} coefficient for bacterioplankton
$Q_{10,n}$	2.0	-	Q_{10} coefficient for nitrification/denitrification
$Q_{10,N5}$	1.49	-	Q_{10} coefficient for dissolution of biogenic silica
T^*	20	°C	Base temperature
E_{PAR}	0.4	-	Fraction of photosynthetically active radiation
λ_w	0.0435	m^{-1}	Background attenuation coefficient
$c_{R^{(2)}}$	0.1×10^{-3}	$\mathrm{m}^2\ (\mathrm{mg\ C})^{-1}$	C-specific attenuation coefficient of particulate detritus
Δz	5.0	m	Depth of surface layer
T^{sum}	28.0	°C	Seawater temperature during the summer
T^{win}	8.0	°C	Seawater temperature during the winter
Q_S^{sum}	20.0	$\mathrm{W\ m}^{-2}$	Incident solar radiation during the summer
Q_S^{win}	300.0	$\mathrm{W\ m}^{-2}$	Incident solar radiation during the winter
S^{sum}	34.0	psu	Seawater salinity during the summer
S^{win}	37.0	psu	Seawater salinity during the winter
W^{sum}	10.0	$\mathrm{m\ s}^{-1}$	Wind speed during the summer
W^{win}	20.0	$\mathrm{m\ s}^{-1}$	Wind speed during the winter

$$\left.\frac{\partial P_{\mathrm{P}}^{(i)}}{\partial t}\right|_{\mathrm{bio}} = \max\left[0, \left.\frac{\partial P_{\mathrm{P}}^{(i)}}{\partial t}\right|_{N^{(1)}}^{\mathrm{upt}}\right] - \sum_{j=1,6} \left.\frac{\partial P_{\mathrm{P}}^{(i)}}{\partial t}\right|_{R_{\mathrm{P}}^{(j)}}^{\mathrm{lys}} - \frac{\partial P_{\mathrm{P}}^{(i)}}{\partial P_{\mathrm{C}}^{(i)}} \sum_{k=3}^{6} \left.\frac{\partial Z_{\mathrm{C}}^{(k)}}{\partial t}\right|_{P_{\mathrm{C}}^{(i)}}^{\mathrm{prd}} \tag{A6}$$

$$\left.\frac{\partial P_{\mathrm{chl}}^{(i)}}{\partial t}\right|_{\mathrm{bio}} = \left.\frac{\partial P_{\mathrm{chl}}^{(i)}}{\partial t}\right|^{\mathrm{syn}} - \frac{\partial P_{\mathrm{chl}}^{(i)}}{\partial P_{\mathrm{C}}^{(i)}} \sum_{j=3}^{6} \left.\frac{\partial Z_{\mathrm{C}}^{(j)}}{\partial t}\right|_{P_{\mathrm{C}}^{(i)}}^{\mathrm{prd}} \tag{A7}$$

$$\left.\frac{\partial P_{\mathrm{S}}^{(i)}}{\partial t}\right|_{\mathrm{bio}} = \left.\frac{\partial P_{\mathrm{S}}^{(i)}}{\partial t}\right|_{N^{(5)}}^{\mathrm{upt}} - \left.\frac{\partial P_{\mathrm{S}}^{(i)}}{\partial t}\right|_{R_{\mathrm{S}}^{(6)}}^{\mathrm{lys}} - \frac{\partial P_{\mathrm{S}}^{(i)}}{\partial P_{\mathrm{C}}^{(i)}} \sum_{j=3}^{6} \left.\frac{\partial Z_{\mathrm{C}}^{(j)}}{\partial t}\right|_{P_{\mathrm{C}}^{(i)}}^{\mathrm{prd}} \text{ if } P_{\mathrm{S}}^{(i)} \exists, \text{ otherwise} \left.\frac{\partial P_{\mathrm{S}}^{(i)}}{\partial t}\right|_{\mathrm{bio}} = 0 \tag{A8}$$

The gross primary production term in the phytoplankton carbon constituent is defined as

$$\left.\frac{\partial P_{\mathrm{C}}^{(i)}}{\partial t}\right|_{O^{(3)}}^{\mathrm{gpp}} = f_P^{(T)} f_P^{(E)} f_P^{(PP)} r_P^{(0)} P_T \tag{A9}$$

https://doi.org/10.5194/egusphere-2025-2901
Preprint. Discussion started: 5 August 2025

where $f_P^{(T)}$ is the temperature regulation factor (Equation (A1)), $f_P^{(E)}$ is the light regulation factor (Equation (A10)), $f_P^{(PP)}$ is the primary production limiting factor (Equation (A11)), $r_P^{(0)}$ is the maximum photosynthetic rate, and P_C is the instantaneous phytoplankton carbon concentration. The light regulation factor is defined as

$$f_P^{(E)} = 1 - \exp\left(- \frac{\alpha_{\text{chl}^{(0)}} E_{\text{PAR}} P_{\text{chl}}}{r_P^{(0)} P_{\text{C}}^{(i)}} \right) \tag{A10}$$

where E_{PAR} is the amount of photosynthetically available radiation (Eq. (A2)) and $\alpha_{\text{chl}^{(0)}}$ is the maximum light utilization coefficient. The primary production limiting factor is defined as

$$f_P^{(PP)} = \min(1.0, \ ) \text{ if } P_{\text{S}}^{(i)} \exists, \text{ otherwise} f_P^{(PP)} = 1.0 \tag{A11}$$

where $N^{(4)}$ and $P_{\text{S}}^{(i)}$ are the instantaneous silicate and phytoplankton silicate concentrations, respectively, $h_P^{(S)}$ is the half saturation constant for silicate limitation, and $\rho_P^{(S)}$ is the half saturation constant for silicate limitation of Contois. Diatoms are the only phytoplankton species that have a silicate constituent ($P_{\text{S}}^{(1)} \exists$ and $P_{\text{S}}^{(2)}$, $P_{\text{S}}^{(3)}$, $P_{\text{S}}^{(4)} \nexists$).

The phytoplankton respiration term includes the basal respiration and activity respiration rates and is defined as

$$\left.\frac{\partial P_{\text{C}}^{(i)}}{\partial t}\right|_{O^{(3)}}^{\text{rsp}} = b_P f_P^{(T)} P_{\text{C}}^{(i)} + \gamma_P \left.\frac{\partial P_{\text{C}}^{(i)}}{\partial t}\right|_{O^{(3)}}^{\text{gpp}} \left\{ 1 - \beta_P - (1 - \beta_P 0 \left[1 - f_P^{(N,P)} \right] \right\} \tag{A12}$$

where b_P is the basal specific respiration rate, γ_P is the activity respiration fraction, β_P is the excreted fraction of primary production, and $f_P^{(N,P)}$ is a multiple nutrient limitation term which allows for the internal storage of nitrogen and phosphorus and is defined as

$$f_P^{(N,P)} = \min\left[f_P^{(N)}, f_P^{(P)} \right] \tag{A13}$$

$$f_P^{(P)} = \min\left\{ 1.0, \max\left[0, \frac{P_{\text{N}}^{(i)} / P_{\text{C}}^{(i)} - \phi_{\text{N}}^{\text{min}}}{\phi_{\text{N}}^{\text{opt}} - \phi_{\text{N}}^{\text{min}}} \right] \right\} \tag{A14}$$

$$f_P^{(P)} = \min\left\{ 1.0, \max\left[0, \frac{P_{\text{P}}^{(i)} / P_{\text{C}}^{(i)} - \phi_{\text{P}}^{\text{min}}}{\phi_{\text{P}}^{\text{opt}} - \phi_{\text{P}}^{\text{min}}} \right] \right\} \tag{A15}$$

where $\phi_{\text{N}}^{\text{min}}$ and $\phi_{\text{P}}^{\text{min}}$ are the minimum phytoplankton quotas and $\phi_{\text{N}}^{\text{opt}}$ and $\phi_{\text{P}}^{\text{opt}}$ are the optimal phytoplankton quotas for nitrogen and phosphorus, respectively.

Phytoplankton lysis includes mortality processes that disrupt the cell membrane due to mechanical, viral, and yeast causes. Cell lysis produces both dissolved and particulate detritus denoted by $R_j^{(1)}$ and $R_j^{(6)}$, respectively, where $j = \text{C, N, P}$. The cytoplasm is released as dissolved detritus, while the structural parts which are less degradable, are released as particulate detritus. The lysis terms for carbon, nitrogen, and phosphorus are defined as

$$\left.\frac{\partial P_{\text{j}}^{(i)}}{\partial t}\right|_{R_{\text{j}}^{(1)}}^{\text{lys}} = \left[1 - \varepsilon_P^{\text{N,P}} \right] \left[\frac{h_P^{(N,P)}}{f_P^{(N,P)} + h_P^{(N,P)}} d_P^{(0)} + \chi^{\text{lys}} \right] P_{\text{j}}^{(i)}, \quad j = \text{C, N, P} \tag{A16}$$

https://doi.org/10.5194/egusphere-2025-2901
Preprint. Discussion started: 5 August 2025

$$\left.\frac{\partial P_{\mathrm{j}}^{(i)}}{\partial t}\right|_{R_{\mathrm{j}}^{(6)}}^{\mathrm{lys}} = \varepsilon_P^{\mathrm{N,P}}\left[\frac{h_P^{(N,P)}}{f_P^{(N,P)}+h_P^{(N,P)}}d_P^{(0)}+\chi^{\mathrm{lys}}\right]P_{\mathrm{j}}^{(i)}\,, \quad j=\mathrm{C,\,N,\,P} \tag{A17}$$

where $h_P^{(N,P)}$ is the nutrient-stress threshold, $d_P^{(0)}$ is the maximum specific nutrient-stress lysis rate, $\varepsilon_P^{\mathrm{N,P}}$ is the fraction of nutrients released as particulate detritus (Equation (A18)), and χ^{lys} is an optional specific lysis rate which is depended on the population density (Equation (A19)). The terms $\varepsilon_P^{\mathrm{N,P}}$ and χ^{lys} are defined as

$$\varepsilon_P^{\mathrm{N,P}} = \min\left[1, \frac{\phi_{\mathrm{N}}^{\min}}{P_{\mathrm{N}}^{(i)}/P_{\mathrm{C}}^{(i)}}, \frac{\phi_{\mathrm{P}}^{\min}}{P_{\mathrm{P}}^{(i)}/P_{\mathrm{C}}^{(i)}}\right] \tag{A18}$$

$$\chi^{\mathrm{lys}} = d_P^{(x)}\frac{P_{\mathrm{C}}^{(i)}}{P_{\mathrm{C}}^{(i)}+h_P^{(x)}} \tag{A19}$$

The exudation term is defined as

$$\left.\frac{\partial P_{\mathrm{C}}^{(i)}}{\partial t}\right|_{R_{\mathrm{C}}^{(2)}}^{\mathrm{exu}} = \left.\frac{\partial P_{\mathrm{C}}^{(i)}}{\partial t}\right|_{O^{(3)}}^{\mathrm{gpp}}\left\{\beta_P+(1-\beta_P)\left[1-f_P^{(N,P)}\right]\right\} \tag{A20}$$

The nitrogen uptake rate is the sum of the uptake of dissolved nitrate, $N^{(3)}$, and ammonium, $N^{(4)}$, and is defined as

$$\sum_{j=3,4}\left.\frac{\partial P_{\mathrm{N}}^{(i)}}{\partial t}\right|_{N^{(j)}}^{\mathrm{upt}} = \min\left\{a_P^{(\mathrm{N})}\left[\frac{h_P^{(\mathrm{N})}}{h_P^{(\mathrm{N})}+N^{(4)}}N^{(3)+N^{(4)}}\right]P_{\mathrm{C}}^{(i)},\ \phi_{\mathrm{N}}^{\max}G_P+\nu_P\left[\phi_{\mathrm{N}}^{\max}-\frac{P_{\mathrm{N}}^{(i)}}{\partial P_{\mathrm{C}}^{(i)}}\right]P_{\mathrm{C}}^{(i)}\right\} \tag{A21}$$

where a_P^{N} is the specific affinity for nitrogen, $h_P^{(N)}$ is the half saturation constant for ammonium uptake, and $\phi_{\mathrm{N}}^{\max}$ is the maximum nitrogen quota. The net primary productivity, G_P, is defined as

$$G_P = \max\left[0, \left.\frac{\partial P_{\mathrm{C}}^{(i)}}{\partial t}\right|_{O^{(3)}}^{\mathrm{gpp}} - \left.\frac{\partial P_{\mathrm{C}}^{(i)}}{\partial t}\right|_{O^{(3)}}^{\mathrm{rsp}} - \left.\frac{\partial P_{\mathrm{N}}^{(i)}}{\partial t}\right|_{R_{\mathrm{N}}^{(1)}}^{\mathrm{lys}} - \left.\frac{\partial P_{\mathrm{N}}^{(i)}}{\partial t}\right|_{R_{\mathrm{N}}^{(6)}}^{\mathrm{lys}} - \left.\frac{\partial P_{\mathrm{C}}^{(i)}}{\partial t}\right|_{R_{\mathrm{C}}^{(2)}}^{\mathrm{exu}}\right] \tag{A22}$$

The specific uptake rate, ν_P, from Equation (A21) is defined as

$$\nu_P = f_P^{(T)}r_P^{(0)} \tag{A23}$$

When the nitrogen uptake rate (Equation (A21)) is positive, the partitioning between dissolved nitrate and ammonium becomes

$$\left.\frac{\partial P_{\mathrm{N}}^{(i)}}{\partial t}\right|_{N^{(3)}}^{\mathrm{upt}} = \varepsilon_P^{(3)}\sum_{j=3,4}\left.\frac{\partial P_{\mathrm{N}}^{(i)}}{\partial t}\right|_{N^{(j)}}^{\mathrm{upt}} \tag{A24}$$

$$\left.\frac{\partial P_{\mathrm{N}}^{(i)}}{\partial t}\right|_{N^{(4)}}^{\mathrm{upt}} = \varepsilon_P^{(4)}\sum_{j=3,4}\left.\frac{\partial P_{\mathrm{N}}^{(i)}}{\partial t}\right|_{N^{(j)}}^{\mathrm{upt}} \tag{A25}$$

https://doi.org/10.5194/egusphere-2025-2901
Preprint. Discussion started: 5 August 2025

where

$$\varepsilon_P^{(3)} = \frac{a_P^{(\mathrm{N})} \frac{h_P^{(\mathrm{N})}}{h_P^{(\mathrm{N})}+N^{(4)}} N^{(3)}}{a_P^{(\mathrm{N})} N^{(4)} + a_P^{(\mathrm{N})} \frac{h_P^{(\mathrm{N})}}{h_P^{(\mathrm{N})}+N^{(4)}} N^{(3)}} \tag{A26}$$

$$\varepsilon_P^{(4)} = \frac{a_P^{(\mathrm{N})} N^{(4)}}{a_P^{(\mathrm{N})} N^{(4)} + a_P^{(\mathrm{N})} \frac{h_P^{(\mathrm{N})}}{h_P^{(\mathrm{N})}+N^{(4)}} N^{(3)}} \tag{A27}$$

When the nitrogen uptake rate (Equation (A21)) is negative, the entire flux goes to the dissolved organic nitrogen pool, $R_{\mathrm{N}}^{(1)}$.

The phosphorus uptake rate is defined as

$$\left.\frac{\partial P_{\mathrm{P}}^{(i)}}{\partial t}\right|_{N^{(1)}}^{\mathrm{upt}} = \min\left\{ a_P^{(P)} N^{(1)} P_{\mathrm{C}}^{(i)},\ \phi_{\mathrm{P}}^{\max} G_P + \nu_P \left[\phi_{\mathrm{P}}^{\max} P_{\mathrm{C}}^{(i)} - P_{\mathrm{P}}^{(i)}\right] \right. \tag{A28}$$

where $a_P^{(P)}$ is the specific affinity constant for phosphorus and $\phi_{\mathrm{P}}^{\max}$ is the maximum phosphorus quota. When the phosphate uptake rate is negative, the entire flux goes to the dissolved organic phosphorus pool, $R_P^{(1)}$.

The net chlorophyll synthesis is defined as

$$\left.\frac{\partial P_{\mathrm{chl}}^{(i)}}{\partial t}\right|^{\mathrm{syn}} = \rho_{\mathrm{chl}}(1-\gamma_P)\left[\left.\frac{\partial P_{\mathrm{C}}^{(i)}}{\partial t}\right|_{O^{(3)}}^{\mathrm{gpp}} - \left.\frac{\partial P_{\mathrm{C}}^{(i)}}{\partial t}\right|_{R_{\mathrm{C}}^{(2)}}^{\mathrm{exu}}\right] - \frac{\partial P_{\mathrm{chl}}^{(i)}}{\partial P_{\mathrm{C}}^{(i)}}\left[\left.\frac{\partial P_{\mathrm{C}}^{(i)}}{\partial t}\right|_{R_{\mathrm{C}}^{(1)}}^{\mathrm{lys}} + \left.\frac{\partial P_{\mathrm{C}}^{(i)}}{\partial t}\right|_{R_{\mathrm{C}}^{(6)}}^{\mathrm{lys}}\right] \tag{A29}$$

where ρ_{chl} is the dynamical chlorophyll to carbon ratio and regulates the amount of chlorophyll in the phytoplankton cell which is defined as

$$\rho_{\mathrm{chl}} = \theta_{\mathrm{chl}}^{(0)} \min\left(1.0, \frac{r_P^{(0)} f_P^{(E)} P_{\mathrm{C}}^{(i)}}{\alpha_{\mathrm{chl}}^{(0)} E_{\mathrm{PAR}} P_{\mathrm{chl}}^{(i)}}\right) \tag{A30}$$

where $\theta_{\mathrm{chl}}^{(0)}$ is the maximum chlorophyll to carbon quota and $\alpha_{\mathrm{chl}}^{(0)}$ is the maximum light utilization coefficient.

Phytoplankton silicate uptake is defined as

$$\left.\frac{\partial P_{\mathrm{S}}^{(i)}}{\partial t}\right|_{N^{(5)}}^{\mathrm{upt}} = \max\left[0,\ \phi_{\mathrm{S}}^{\mathrm{opt}}\left(\left.\frac{\partial P_{\mathrm{C}}^{(i)}}{\partial t}\right|_{O^{(3)}}^{\mathrm{gpp}} - b_P f_P^{(T)} P_{\mathrm{C}}^{(i)}\right)\right] \tag{A31}$$

where $\phi_{\mathrm{S}}^{\mathrm{opt}}$ is the optimal silicate to carbon ratio in silicifiers. Phytoplankton silicate loss associated with lysis is defined as

$$\left.\frac{\partial P_{\mathrm{S}}^{(i)}}{\partial t}\right|_{R_{\mathrm{S}}^{(6)}}^{\mathrm{lys}} = \frac{\partial P_{\mathrm{S}}^{(i)}}{\partial P_{\mathrm{C}}^{(i)}}\left[\left.\frac{\partial P_{\mathrm{N}}^{(i)}}{\partial t}\right|_{R_{\mathrm{N}}^{(1)}}^{\mathrm{lys}} + \left.\frac{\partial P_{\mathrm{N}}^{(i)}}{\partial t}\right|_{R_{\mathrm{N}}^{(6)}}^{\mathrm{lys}}\right] \tag{A32}$$

The phytoplankton predation terms are presented with the zooplankton equations in Section A2.3.

https://doi.org/10.5194/egusphere-2025-2901
Preprint. Discussion started: 5 August 2025

Table A5. Symbols, values, units, and descriptions for the phytoplankton parameters within the BFM

Symbol	$P^{(1)}$	$P^{(2)}$	$P^{(3)}$	$P^{(4)}$	Units	Description
$c_P^{(T)}$	0.0	0.0	0.0	0.0	-	Cut-off threshold for temperature regulating factor
$r_P^{(0)}$	2.5	1.6	1.02	0.83	d^{-1}	Maximum specific photosynthetic rate
b_P	0.05	0.05	0.05	0.1	d^{-1}	Basal specific respiration rate
$d_P^{(0)}$	0.01	0.05	0.01	0.02	d^{-1}	Maximum specific nutrient-stress lysis rate
γ_P	0.1	0.05	0.2	0.1	-	Activity respiration factor
β_P	0.01	0.05	0.1	0.15	-	Excreted fraction of primary production
$h_P^{(N,P)}$	0.1	0.1	0.1	0.5	-	Nutrient stress threshold
$h_P^{(x)}$	0.0	0.0	0.0	100.0	mg C m^{-3}	Half saturation constant for extra lysis
$h_P^{(N)}$	1.0	1.5	0.1	1.0	mmol N-NH_4 m^{-3}	Half saturation constant for ammonium uptake
$d_P^{(x)}$	0.0	0.0	0.0	0.5	d^{-1}	Extra lysis rate
$a_P^{(N)}$	0.025	0.025	0.025	0.025	m^3 (mg C)$^{-1}$ d^{-1}	Specific affinity constant for nitrogen
$a_P^{(P)}$	2.5×10^{-3}	2.5×10^{-3}	2.5×10^{-3}	2.5×10^{-3}	m^3 (mg C)$^{-1}$ d^{-1}	Specific affinity constant for phosphorus
$a_P^{(S)}$	0.0	0.0	0.0	0.0	m^3 (mg C)$^{-1}$ d^{-1}	Specific affinity constant for silicate
$\phi_N^{(\min)}$	6.87×10^{-3}	6.87×10^{-3}	6.87×10^{-3}	6.87×10^{-3}	mmol N (mg C)$^{-1}$	Minimum nitrogen quota
$\phi_N^{(\text{opt})}$	1.26×10^{-2}	1.26×10^{-2}	1.26×10^{-2}	1.26×10^{-2}	mmol N (mg C)$^{-1}$	Optimal nitrogen quota
$\phi_N^{(\max)}$	1.26×10^{-2}	1.26×10^{-2}	1.26×10^{-2}	1.26×10^{-2}	mmol N (mg C)$^{-1}$	Maximum nitrogen quota
$\phi_P^{(\min)}$	4.29×10^{-4}	4.29×10^{-4}	4.29×10^{-4}	4.29×10^{-4}	mmol P (mg C)$^{-1}$	Minimum phosphorus quota
$\phi_P^{(\text{opt})}$	7.86×10^{-4}	7.86×10^{-4}	7.86×10^{-4}	7.86×10^{-4}	mmol P (mg C)$^{-1}$	Optimum phosphorus quota
$\phi_P^{(\max)}$	1.572×10^{-3}	7.86×10^{-4}	1.572×10^{-3}	1.572×10^{-3}	mmol P (mg C)$^{-1}$	Maximum phosphorus quota
$\phi_S^{(\min)}$	0.0	0.0	0.0	0.0	mmol Si (mg C)$^{-1}$	Minimum Si:C ratio in silicifiers
$\phi_S^{(\text{opt})}$	0.01	0.0	0.0	0.0	mmol Si (mg C)$^{-1}$	Optimal Si:C ratio in silicifiers
$\theta_{chl}^{(0)}$	0.035	0.016	0.02	0.035	mg chl (mg C)$^{-1}$	Maximum chl:C quotum
$\alpha_{\text{chl}}^{(0)}$	1.1×10^{-5}	1.52×10^{-5}	0.7×10^{-5}	0.68×10^{-5}	mg C (mg chl)$^{-1}$ μE^{-1} m^2	Maximum light utilization coefficient
c_P	0.03	0.03	0.03	0.03	m^2 (mg chl)$^{-1}$	Chlorophyll-specific light absorption coefficient
$h_P^{(S)}$	1.0	0.0	0.0	0.0	mmol Si m^{-3}	Half saturation constant for Si-limitation
$\rho_P^{(S)}$	0.0	0.0	0.0	0.0	-	Half saturation constant for Si-limitation of Contois

A2.2 Bacterioplankton

Bacteria are part of the living organic CFF and have carbon, nitrogen, and phosphorus constituents, each representing a different state variable. The bacteria rate equations are

$$\left.\frac{\partial B_{\text{C}}}{\partial t}\right|_{\text{bio}} = \sum_{i=1,2,3,6} \left.\frac{\partial B_{\text{C}}}{\partial t}\right|^{\text{upt}}_{R_{\text{C}}^{(i)}} - \left.\frac{\partial B_{\text{C}}}{\partial t}\right|^{\text{rsp}}_{O^{(3)}} - \sum_{j=2,3} \left.\frac{\partial B_{\text{C}}}{\partial t}\right|^{\text{rel}}_{R_{\text{C}}^{(j)}} - \sum_{k=1,6} \left.\frac{\partial B_{\text{C}}}{\partial t}\right|^{\text{lys}}_{R_{\text{C}}^{(k)}} - \sum_{m=5,6} \left.\frac{\partial B_{\text{C}}}{\partial t}\right|^{\text{prd}}_{R_{\text{C}}^{(m)}} \tag{A33}$$

$$\left.\frac{\partial B_{\text{N}}}{\partial t}\right|_{\text{bio}} = \sum_{i=1,6} \left.\frac{\partial B_{\text{N}}}{\partial t}\right|^{\text{upt}}_{R_{\text{N}}^{(i)}} + \left.\frac{\partial B_{\text{N}}}{\partial t}\right|^{\text{upt,rel}}_{\text{N}^{(4)}} - \sum_{j=1,6} \left.\frac{\partial B_{\text{C}}}{\partial t}\right|^{\text{lys}}_{R_{\text{C}}^{(j)}} - \frac{B_{\text{N}}}{B_{\text{N}}} \sum_{k=5,6} \left.\frac{\partial Z_{\text{C}}^{(k)}}{\partial t}\right|^{\text{prd}}_{B_{\text{C}}} \tag{A34}$$

$$\left.\frac{\partial B_{\text{P}}}{\partial t}\right|_{\text{bio}} = \sum_{i=1,6} \left.\frac{\partial B_{\text{P}}}{\partial t}\right|^{\text{upt}}_{R_{\text{P}}^{(i)}} + \left.\frac{\partial B_{\text{P}}}{\partial t}\right|^{\text{upt,rel}}_{\text{N}^{(1)}} - \sum_{j=1,6} \left.\frac{\partial B_{\text{C}}}{\partial t}\right|^{\text{lys}}_{R_{\text{P}}^{(j)}} - \frac{B_{\text{P}}}{B_{\text{C}}} \sum_{k=5,6} \left.\frac{\partial Z_{\text{C}}^{(k)}}{\partial t}\right|^{\text{prd}}_{B_{\text{C}}} \tag{A35}$$

https://doi.org/10.5194/egusphere-2025-2901
Preprint. Discussion started: 5 August 2025

Bacteria lysis of dissolved and particulate matter for carbon, nitrogen, and phosphorus are defined as

$$\left.\frac{\partial B_{\mathrm{C}}}{\partial t}\right|_{R_{\mathrm{C}}^{(1)}}^{\mathrm{lys}} = \varepsilon_i \left(\frac{B_{\mathrm{i}}}{B_{\mathrm{C}}}\right)\left(d_B^{(0)} f_B^{(T)} + d_B^{(d)} B_{\mathrm{C}}\right) B_{\mathrm{C}}, \quad i = \mathrm{C, N, P} \tag{A36}$$

$$\left.\frac{\partial B_{\mathrm{C}}}{\partial t}\right|_{R_{\mathrm{C}}^{(1)}}^{\mathrm{lys}} = (1-\varepsilon_i)\left(\frac{B_{\mathrm{i}}}{B_{\mathrm{C}}}\right)\left(d_B^{(0)} f_B^{(T)} + d_B^{(d)} B_{\mathrm{C}}\right) B_{\mathrm{C}}, \quad i = \mathrm{C, N, P} \tag{A37}$$

where ε_i is the partition between dissolved and particulate excretion of either carbon, nitrogen, or phosphorus, $d_B^{(0)}$ is the specific mortality rate, $d_B^{(d)}$ is the density-dependent specific mortality rate, and $f_B^{(T)}$ is the temperature regulation factor (Equation (A1)). The uptake of dissolved organic carbon is defined as

$$\left.\frac{\partial B_{\mathrm{C}}}{\partial t}\right|_{R_{\mathrm{C}}^{(1)}}^{\mathrm{upt}} = \frac{\min\left(f_B^{(N,P)} f_B^{(T)} r_B^{(0)} B_{\mathrm{C}},\ \sum_{j=1,6} \nu_B^{(R^{(j)})} f_{(R^{(j)})}^{(N,P)} R_{\mathrm{C}}^{(j)}\right) \nu_B^{(R^{(1)})} f_{(R^{(1)})}^{(N,P)} R_{\mathrm{C}}^{(1)}}{\sum_{j=1,6} \nu_B^{(R^{(j)})} f_{(R^{(j)})}^{(N,P)} R_{\mathrm{C}}^{(j)}} \tag{A38}$$

where $f_B^{(N,P)}$ is a non-dimensional regulating factor for the nutritional content of bacterial cells (), $r_B^{(0)}$ is the maximum specific growth rate, $\nu_B^{(R^{(j)})}$ is the specific uptake rate for substrate, and $f_{(R^{(j)})}^{(N,P)}$ is a non-dimensional regulating factor for organic substrate (Equation (A44)). Similarly to Equation (A38), the uptake of particulate organic carbon is defined as

$$\left.\frac{\partial B_{\mathrm{C}}}{\partial t}\right|_{R_{\mathrm{C}}^{(6)}}^{\mathrm{upt}} = \frac{\min\left(f_B^{(N,P)} f_B^{(T)} r_B^{(0)} B_{\mathrm{C}},\ \sum_{j=1,6} \nu_B^{(R^{(j)})} f_{(R^{(j)})}^{(N,P)} R_{\mathrm{C}}^{(j)}\right) \nu_B^{(R^{(6)})} f_{(R^{(6)})}^{(N,P)} R_{\mathrm{C}}^{(6)}}{\sum_{j=1,6} \nu_B^{(R^{(j)})} f_{(R^{(j)})}^{(N,P)} R_{\mathrm{C}}^{(j)}} \tag{A39}$$

Since the parameters $\nu_B^{(R^{(2)})}$ and $\nu_B^{(R^{(3)})}$ are both zero, the uptake of semi-labile dissolved organic carbon and semi-refractory dissolved organic carbon are both zero.

$$\left.\frac{\partial B_{\mathrm{C}}}{\partial t}\right|_{R_{\mathrm{C}}^{(j)}}^{\mathrm{upt}} = 0, \quad j = 2, 3 \tag{A40}$$

The release of semi-labile dissolved organic carbon and semi-refractory dissolved organic carbon are defined by

$$\left.\frac{\partial B_{\mathrm{C}}}{\partial t}\right|_{R_{\mathrm{C}}^{(2)}}^{\mathrm{rel}} = \max\left(0,\ 1-f_B^{(N)},\ 1-f_B^{(P)}\right) \nu_B^{(\mathrm{C})} B_{\mathrm{C}} \tag{A41}$$

$$\left.\frac{\partial B_{\mathrm{C}}}{\partial t}\right|_{R_{\mathrm{C}}^{(3)}}^{\mathrm{rel}} = \min\left(f_B^{(N,P)} f_B^{(T)} r_B^{(0)} B_{\mathrm{C}},\ \sum_{j=1,6} \nu_B^{(R^{(j)})} f_{(R^{(j)})}^{(N,P)} R_{\mathrm{C}}^{(j)}\right)\left(1-\gamma_B^a\right)\gamma_B^a\ \beta_B \tag{A42}$$

where ν_B^{C} is the specific relaxation rate for semi-labile carbon release, γ_B^a is the activity respiration fraction, and β_B is the fractional excretion of semi-refractory carbon.

https://doi.org/10.5194/egusphere-2025-2901
Preprint. Discussion started: 5 August 2025

The non-dimensional regulating factors from Equations (A38) and (A39) are defined as

$$f_B^{(N,P)} = \min\left(1,\ \frac{B_\mathrm{N}/B_\mathrm{C}}{\psi_\mathrm{N}^{(\mathrm{opt})}},\ \frac{B_\mathrm{P}/B_\mathrm{C}}{\psi_\mathrm{N}^{(\mathrm{opt})}}\right) \tag{A43}$$

$$f_{R^{(j)}}^{(N,P)} = \min\left(1,\ \frac{R_\mathrm{N}^{(j)}/R_\mathrm{C}^{(j)}}{\psi_\mathrm{N}^{(\mathrm{opt})}},\ \frac{R_\mathrm{P}^{(j)}/R_\mathrm{C}^{(j)}}{\psi_\mathrm{P}^{(\mathrm{opt})}}\right), \quad j = 1,6 \tag{A44}$$

where $\psi_\mathrm{N}^{(\mathrm{opt})}$ and $\psi_\mathrm{N}^{(\mathrm{opt})}$ are the optimal bacteria quotas for nitrogen and phosphorus, respectively. The uptake of dissolved and particulate organic nutrient components can be computed using the nutrient rations of organic matter.

$$\left.\frac{\partial B_\mathrm{i}}{\partial t}\right|_{R_\mathrm{i}^{(j)}}^{\mathrm{upt}} = \frac{R_\mathrm{i}^{(j)}}{R_\mathrm{C}^{(j)}} \left.\frac{\partial B_\mathrm{i}}{\partial t}\right|_{R_\mathrm{C}^{(j)}}^{\mathrm{upt}}, \quad i = \mathrm{N,\,P};\ j = 1,6 \tag{A45}$$

The nutrient uptake and release of ammonium and phosphate are defined as

$$\left.\frac{\partial B_\mathrm{N}}{\partial t}\right|_{\mathrm{N}^{(4)}}^{\mathrm{upt,rel}} = f_B^{(N)} \nu_B^{(N)} \left(\frac{B_\mathrm{N}}{B_\mathrm{C}} - \psi_\mathrm{N}^{(\mathrm{opt})}\right) B_\mathrm{C} \tag{A46}$$

$$\left.\frac{\partial B_\mathrm{P}}{\partial t}\right|_{\mathrm{N}^{(1)}}^{\mathrm{upt,rel}} = f_B^{(P)} \nu_B^{(P)} \left(\frac{B_\mathrm{P}}{B_\mathrm{C}} - \psi_\mathrm{P}^{(\mathrm{opt})}\right) B_\mathrm{C} \tag{A47}$$

where $\nu_B^{(\mathrm{N})}$ and $\nu_B^{(\mathrm{P})}$ are specific relaxation rates towards the optimal internal quota. The non-dimensional factors $f_B^{(N)}$ and $f_B^{(P)}$ are defined as

$$f_B^{(N,P)} = \begin{cases} -1\,, & \text{if } \frac{B_\mathrm{N,P}}{B_\mathrm{C}} - \psi_\mathrm{N,P}^{(\mathrm{opt})} > 0 \\ \frac{N^{(4,1)}}{N^{(4,1)} + h_B^{(\mathrm{N,P})}}\,, & \text{if } \frac{B_\mathrm{N,P}}{B_\mathrm{C}} - \psi_\mathrm{N,P}^{(\mathrm{opt})} < 0 \end{cases} \tag{A48}$$

The bacteria respiration term is defined as

$$\left.\frac{\partial B_\mathrm{C}}{\partial t}\right|_{O^{(3)}}^{\mathrm{rsp}} = b_B f_B^{(T)} B_\mathrm{C} + \left[\gamma_B^{(a)} + \gamma_B^{(O)} - \left(1 - f_B^{(O)}\right)\right] \sum_{j=1,6} \left.\frac{\partial B_\mathrm{C}}{\partial t}\right|_{R_\mathrm{C}^{(j)}}^{\mathrm{upt}} \tag{A49}$$

where b_B is the basal specific respiration rate, $\gamma_B^{(a)}$ is the activity respiration fraction, $\gamma_B^{(O)}$ is the additional respiration fraction under anoxic conditions. The non-dimensional regulating factor for oxygen, $f_B^{(O)}$, is defined as

$$f_B^{(O)} = \frac{\left(O^{(2)}\right)^3}{\left(O^{(2)}\right)^3 + \left(h_B^{(O)}\right)^3} \tag{A50}$$

where $h_B^{(O)}$ is the half saturation value for oxygen limitation.

The bacteria predation terms are presented with the zooplankton equations in Section A2.3.

https://doi.org/10.5194/egusphere-2025-2901
Preprint. Discussion started: 5 August 2025

Table A6. Symbols, values, units, and descriptions for bacteria parameters within BFM.

Symbol	Value	Units	Description
$h_B^{(O)}$	30.0	mmol O_2 m^{-3}	Half saturation value for oxygen limitation
$r_B^{(O)}$	8.38	d^{-1}	Potential specific growth rate
b_B	0.1	d^{-1}	Basal specific respiration rate
$\gamma_B^{(a)}$	0.6	-	Activity respiration fraction
$\gamma_B^{(O)}$	0.2	-	Additional respiration fraction under anoxic conditions
$d_B^{(0)}$	0.1	d^{-1}	Specific mortality rate
$d_B^{(d)}$	0.0	m^3 (mg C)$^{-1}$ d^{-1}	Density-dependent specific mortality rate
$\nu_B^{(R^{(1)})}$	0.3	d^{-1}	Specific quality-dependent potential $R^{(1)}$ uptake (nutrient-rich labile)
$\nu_B^{(R^{(2)})}$	0.0	d^{-1}	Specific potential $R^{(2)}$ uptake (semi-labile)
$\nu_B^{(R^{(3)})}$	0.0	d^{-1}	Specific potential $R^{(3)}$ uptake (semi-refractory)
$\nu_B^{(R^{(6)})}$	0.01	d^{-1}	Specific potential $R^{(6)}$ uptake (particulate)
$a_B^{(N)}$	0.0	m^3 (mg C)$^{-1}$ d^{-1}	Specific affinity constant for nitrogen
$a_B^{(P)}$	0.0	m^3 (mg C)$^{-1}$ d^{-1}	Specific affinity constant for phosphorus
$\nu_B^{(C)}$	1.0	d^{-1}	Relaxation time scales for semi-labile carbon release
$\nu_B^{(N)}$	1.0	d^{-1}	Relaxation time scales for nitrogen uptake or remineralization
$\nu_B^{(P)}$	1.0	d^{-1}	Relaxation time scales for phosphorus uptake or remineralization
$\psi_{\mathrm{N}}^{(\mathrm{min})}$	1.67×10^{-2}	mmol N (mg C)$^{-1}$	Minimum nitrogen quota
$\psi_{\mathrm{N}}^{(\mathrm{opt})}$	1.67×10^{-2}	mmol N (mg C)$^{-1}$	Optimal nitrogen quota
$\psi_{\mathrm{P}}^{(\mathrm{min})}$	1.85×10^{-3}	mmol P (mg C)$^{-1}$	Minimum phosphorus quota
$\psi_{\mathrm{P}}^{(\mathrm{opt})}$	1.85×10^{-3}	mmol P (mg C)$^{-1}$	Optimal phosphorus quota
$h_B^{(N)}$	5.0	mmol N (mg C)$^{-1}$	Half saturation for nitrogen uptake
$h_B^{(P)}$	1.0	mmol P (mg C)$^{-1}$	Half saturation for phosphorus uptake
β_B	0.0	-	Fractional excretion of $R^{(3)}$ uptake (semi-refractory)

A2.3 Zooplankton

Zooplankton are part of the living organic CFF and the BFM contains 4 different zooplankton species: carnivorous mesozooplankton, omnivorous mesozooplankton, mircozooplankton, and heterotrophic nanoflagellates. Each zooplankton species has carbon, nitrogen, and phosphorus constituents, each representing a different state variable. The zooplankton rate equations are

$$\left.\frac{\partial Z_{\mathrm{C}}^{(i)}}{\partial t}\right|_{\mathrm{bio}} = \left.\frac{\partial Z_{\mathrm{C}}^{(i)}}{\partial t}\right|_{B_{\mathrm{C}}}^{\mathrm{prd}} + \sum_{j=1}^{4} \left.\frac{\partial Z_{\mathrm{C}}^{(i)}}{\partial t}\right|_{P_{\mathrm{C}}^{(j)}}^{\mathrm{prd}} + \sum_{k=3}^{6} \left.\frac{\partial Z_{\mathrm{C}}^{(i)}}{\partial t}\right|_{Z_{\mathrm{C}}^{(k)}}^{\mathrm{prd}} - \sum_{k=3}^{6} \left.\frac{\partial Z_{\mathrm{C}}^{(k)}}{\partial t}\right|_{Z_{\mathrm{C}}^{(i)}}^{\mathrm{prd}} - \sum_{m=1,6} \left.\frac{\partial Z_{\mathrm{C}}^{(i)}}{\partial t}\right|_{R_{\mathrm{C}}^{(m)}}^{\mathrm{rel}} - \left.\frac{\partial Z_{\mathrm{C}}^{(i)}}{\partial t}\right|_{O^{(3)}}^{\mathrm{rsp}} \tag{A51}$$

https://doi.org/10.5194/egusphere-2025-2901
Preprint. Discussion started: 5 August 2025

$$\left.\frac{\partial Z_{\mathrm{N}}^{(i)}}{\partial t}\right|_{\mathrm{bio}} = \frac{B_{\mathrm{N}}}{B_{\mathrm{C}}}\frac{\partial Z_{\mathrm{C}}^{(i)}}{\partial t}\bigg|_{B_{\mathrm{C}}}^{\mathrm{prd}} + \sum_{j=1}^{4}\frac{P_{\mathrm{N}}^{(j)}}{P_{\mathrm{C}}^{(j)}}\frac{\partial Z_{\mathrm{C}}^{(i)}}{\partial t}\bigg|_{P_{\mathrm{C}}^{(j)}}^{\mathrm{prd}} + \sum_{k=3}^{6}\frac{Z_{\mathrm{N}}^{(k)}}{Z_{\mathrm{C}}^{(k)}}\frac{\partial Z_{\mathrm{C}}^{(i)}}{\partial t}\bigg|_{Z_{\mathrm{C}}^{(k)}}^{\mathrm{prd}} - \sum_{k=3}^{6}\frac{Z_{\mathrm{N}}^{(i)}}{Z_{\mathrm{C}}^{(i)}}\frac{\partial Z_{\mathrm{C}}^{(k)}}{\partial t}\bigg|_{Z_{\mathrm{C}}^{(i)}}^{\mathrm{prd}} - \sum_{m=1,6}\frac{\partial Z_{\mathrm{N}}^{(i)}}{\partial t}\bigg|_{R_{\mathrm{N}}^{(m)}}^{\mathrm{rel}} - \frac{\partial Z_{\mathrm{N}}^{(i)}}{\partial t}\bigg|_{N^{(4)}}^{\mathrm{rel}} \tag{A52}$$

$$\left.\frac{\partial Z_{\mathrm{P}}^{(i)}}{\partial t}\right|_{\mathrm{bio}} = \frac{B_{\mathrm{P}}}{B_{\mathrm{C}}}\frac{\partial Z_{\mathrm{C}}^{(i)}}{\partial t}\bigg|_{B_{\mathrm{C}}}^{\mathrm{prd}} + \sum_{j=1}^{4}\frac{P_{\mathrm{P}}^{(j)}}{P_{\mathrm{C}}^{(j)}}\frac{\partial Z_{\mathrm{C}}^{(i)}}{\partial t}\bigg|_{P_{\mathrm{C}}^{(j)}}^{\mathrm{prd}} + \sum_{k=3}^{6}\frac{Z_{\mathrm{P}}^{(k)}}{Z_{\mathrm{C}}^{(k)}}\frac{\partial Z_{\mathrm{C}}^{(i)}}{\partial t}\bigg|_{Z_{\mathrm{C}}^{(k)}}^{\mathrm{prd}} - \sum_{k=3}^{6}\frac{Z_{\mathrm{P}}^{(i)}}{Z_{\mathrm{C}}^{(i)}}\frac{\partial Z_{\mathrm{C}}^{(k)}}{\partial t}\bigg|_{Z_{\mathrm{C}}^{(i)}}^{\mathrm{prd}} - \sum_{m=1,6}\frac{\partial Z_{\mathrm{P}}^{(i)}}{\partial t}\bigg|_{R_{\mathrm{N}}^{(m)}}^{\mathrm{rel}} - \frac{\partial Z_{\mathrm{P}}^{(i)}}{\partial t}\bigg|_{N^{(1)}}^{\mathrm{rel}} \tag{A53}$$

The total amount of food available to zooplankton groups considering the set of possible preys, $X_i \in \left\{P_i^{(j)}, B_i, Z_i^{(j)}\right\}$, is defined as

$$F_i = \sum_X \delta_{Z,X} e_{Z,X} X_i \tag{A54}$$

where $\delta_{Z,X}$ is the availability of prey X_i for predator Z. The non-dimensional capture efficiency, $e_{Z,X}$, is defined as

$$e_{Z,X} = \frac{X_{\mathrm{C}}}{X_{\mathrm{C}} + \mu_Z} \tag{A55}$$

where μ_Z is the feeding threshold.

The total carbon ingestion of zooplankton is defined as

$$\left.\frac{\partial Z_{\mathrm{i}}}{\partial t}\right|_{X_{\mathrm{i}}}^{\mathrm{prd}} = f_Z^{(T)} r_Z^{(0)} \frac{\delta_{Z,X} e_{Z,X} X_{\mathrm{i}}}{F_{\mathrm{i}}} \frac{F_{\mathrm{i}}}{F_{\mathrm{i}} + h_Z^F} Z_{\mathrm{C}} \tag{A56}$$

where $\delta_{Z,X}$ is the availability of prey X_i for predator Z, $e_{Z,X}$ is the non-dimensional capture efficiency, $f_Z^{(T)}$ is the temperature regulation factor (Equation (A1), F_{i} is the prey for predator Z, and $Z_{\mathrm{i}}^{(i)}$ is the instantaneous zooplankton concentration for $i = \mathrm{C}, \mathrm{N}, \mathrm{P}$. The specific search volume, h_Z^F, is defined as

$$h_Z^F = \frac{r_{0_Z}}{\nu_Z} \tag{A57}$$

where r_{0_Z} and ν_Z are the specific growth rate and specific search volume for zooplankton, respectively. The total ingestion rate for carbon, nitrogen, and phosphorus is defined as

$$I_j = \sum_X \left.\frac{\partial Z_{\mathrm{j}}}{\partial t}\right|_{X_{\mathrm{j}}}^{\mathrm{prd}}, \quad j = \mathrm{C}, \mathrm{N}, \mathrm{P} \tag{A58}$$

The terms in the rate equations are defined differently for mesozooplankton ($Z^{(3)}$,$Z^{(4)}$) and microzooplankton ($Z^{(5)}$,$Z^{(6)}$) and are outlined separately in the following sections.

https://doi.org/10.5194/egusphere-2025-2901
Preprint. Discussion started: 5 August 2025

Table A7. Prey availability for zooplankton predation terms within the BFM. These parameters are unitless.

Symbol	$Z^{(3)}$	$Z^{(4)}$	$Z^{(5)}$	$Z^{(6)}$
$\delta_{Z^{(i)},P^{(1)}}$	0.0	1.0	0.5	0.0
$\delta_{Z^{(i)},P^{(2)}}$	0.0	0.1	1.0	0.1
$\delta_{Z^{(i)},P^{(3)}}$	0.0	0.0	0.5	1.0
$\delta_{Z^{(i)},P^{(4)}}$	0.0	0.7	0.0	0.0

A2.3.1 Mesozooplankton

The respiration term is defined as

$$\left.\frac{\partial Z_{\mathrm{C}}^{(i)}}{\partial t}\right|_{O^{(3)}}^{\mathrm{rsp}} = I_{\mathrm{C}}\left(1-\eta_Z-\beta_Z\right)+b_Z f_Z^{(T)} Z_{\mathrm{C}}^{(i)} \tag{A59}$$

where I_{C} is the total ingestion rate for carbon, η_Z is the assimilation efficiency, β_Z is the excreted fraction of uptake, b_Z is the basal specific respiration rate, $f_Z^{(T)}$ is the temperature regulation factor (Equation (A1), and $Z_{\mathrm{C}}^{(i)}$ is the instantaneous zooplankton carbon concentration.

Mesozooplankton are assumed to have no dissolved products.

$$\left.\frac{\partial Z_{\mathrm{j}}^{(i)}}{\partial t}\right|_{R_{\mathrm{j}}^{(1)}}^{\mathrm{rel}} = 0, \quad j = \mathrm{C, N, P} \tag{A60}$$

The particulate organic carbon release term is defined as

$$\left.\frac{\partial Z_{\mathrm{C}}^{(i)}}{\partial t}\right|_{R_{\mathrm{C}}^{(6)}}^{\mathrm{rel}} = I_{\mathrm{C}}\beta_Z + d_Z^{(\mathrm{dns})}\left(1-f_Z^{(O)}\right) f_Z^{(T)} Z_{\mathrm{C}}^{(i)} + d_Z\left(Z_{\mathrm{C}}^{(i)}\right)^{\gamma_Z} + Q_Z^{(\mathrm{C})} \tag{A61}$$

where $d_Z^{(\mathrm{dns})}$ is the density-dependent specific mortality rate, $f_Z^{(O)}$ is the oxygen-dependent regulation factor (Equation (A62)), d_Z is the specific mortality rate, γ_Z is the exponent for density-dependent mortality, and $Q_Z^{(\mathrm{C})}$ is a correction term for carbon that eliminates the excess of the non-limiting constituent. The oxygen-dependent regulation factor is defined as

$$f_Z^{(O)} = \frac{\left(O^{(2)}\right)^3}{\left(O^{(2)}\right)^3 + \left(h_Z^{(O)}\right)^3} \tag{A62}$$

where $h_Z^{(O)}$ is the half saturation value for oxygen.

The particulate organic nitrogen and phosphorus release terms are defined as

$$\left.\frac{\partial Z_{\mathrm{j}}^{(i)}}{\partial t}\right|_{R_{\mathrm{j}}^{(6)}}^{\mathrm{rel}} = I_j\beta_Z + \frac{Z_{\mathrm{j}}^{(i)}}{Z_{\mathrm{C}}^{(i)}}\left[d_Z^{(\mathrm{dns})}\left(1-f_Z^{(O)}\right) f_Z^{(T)} Z_{\mathrm{C}}^{(i)} + d_Z\left(Z_{\mathrm{C}}^{(i)}\right)^{\gamma_Z}, \quad j = \mathrm{N, P}\right. \tag{A63}$$

https://doi.org/10.5194/egusphere-2025-2901
Preprint. Discussion started: 5 August 2025

where I_j is the total ingestion rate for either nitrogen or phosphorus.

The release of ammonium and phosphate are defined as

$$\left.\frac{\partial Z_{\mathrm{N}}^{(i)}}{\partial t}\right|_{N^{(4)}}^{\mathrm{rel}} = b_Z f_Z^{(O)} f_Z^{(T)} Z_{\mathrm{N}}^{(i)} + Q_Z^{\mathrm{N}} \tag{A64}$$

$$\left.\frac{\partial Z_{\mathrm{P}}^{(i)}}{\partial t}\right|_{N^{(1)}}^{\mathrm{rel}} = b_Z f_Z^{(O)} f_Z^{(T)} Z_{\mathrm{P}}^{(i)} + Q_Z^{\mathrm{P}} \tag{A65}$$

where Q_Z^{N} and Q_Z^{P} are correction terms that eliminate the excess of the non-limiting constituent. The values for these correction terms are determined by a switch which indicates whether carbon, nitrogen, or phosphorus is the limiting nutrient. Then the correction terms are calculated using the information in Table A8. The switch uses the actual elemental ratios of ingested material which are defined by

$$\Gamma_Z^{(j)} = \frac{\left(1-\beta_Z\right) I_j}{\eta_Z I_{\mathrm{C}}}, \quad j = \mathrm{N}, \mathrm{P} \tag{A66}$$

Table A8. Mesozooplankton method of eliminating the excess of the non-limiting constituent. The switch determines whether carbon, nitrogen, or phosphorus is the limiting nutrient.

Limiting Element	**Carbon**	**Nitrogen**	**Phosphorus**
Switch	default	if $\frac{\Gamma_Z^{(\mathrm{N})}}{Z_{(\mathrm{N})}^{(i)}/Z_{(\mathrm{C})}^{(i)}} < \frac{\Gamma_Z^{(\mathrm{P})}}{Z_{(\mathrm{P})}^{(i)}/Z_{(\mathrm{C})}^{(i)}}$ or $\left\lvert \frac{\Gamma_Z^{(\mathrm{N})}}{Z_{(\mathrm{N})}^{(i)}/Z_{(\mathrm{C})}^{(i)}} - \frac{\Gamma_Z^{(\mathrm{P})}}{Z_{(\mathrm{P})}^{(i)}/Z_{(\mathrm{C})}^{(i)}} \right\rvert < 0$ and $\Gamma_Z^{(\mathrm{N})} < Z_{(\mathrm{N})}^{(i)}/Z_{(\mathrm{C})}^{(i)}$	if $\frac{\Gamma_Z^{(\mathrm{P})}}{Z_{(\mathrm{P})}^{(i)}/Z_{(\mathrm{C})}^{(i)}} < \frac{\Gamma_Z^{(\mathrm{N})}}{Z_{(\mathrm{N})}^{(i)}/Z_{(\mathrm{C})}^{(i)}}$ or $\left\lvert \frac{\Gamma_Z^{(\mathrm{P})}}{Z_{(\mathrm{P})}^{(i)}/Z_{(\mathrm{C})}^{(i)}} - \frac{\Gamma_Z^{(\mathrm{N})}}{Z_{(\mathrm{N})}^{(i)}/Z_{(\mathrm{C})}^{(i)}} \right\rvert < 0$ and $\Gamma_Z^{(\mathrm{P})} < Z_{(\mathrm{P})}^{(i)}/Z_{(\mathrm{C})}^{(i)}$
$Q_Z^{(\mathrm{C})}$	0	$\eta_Z I_{\mathrm{C}} - \frac{(1-\beta_Z)}{\psi_{\mathrm{N}}^{(opt)}} I_{\mathrm{N}}$	$\eta_Z I_{\mathrm{C}} - \frac{(1-\beta_Z)}{\psi_{\mathrm{P}}^{(opt)}} I_{\mathrm{P}}$
$Q_Z^{(\mathrm{N})}$	$(1-\beta_Z) I_{\mathrm{N}} - \psi_{\mathrm{N}}^{(opt)} \eta_Z I_{\mathrm{C}}$	0	$(1-\beta_Z) I_{\mathrm{N}} - \psi_{\mathrm{N}}^{(opt)} (\eta_Z I_{\mathrm{C}} - Q_Z^{(\mathrm{C})})$
$Q_Z^{(\mathrm{P})}$	$(1-\beta_Z) I_{\mathrm{P}} - \psi_{\mathrm{P}}^{(opt)} \eta_Z I_{\mathrm{C}}$	$(1-\beta_Z) I_{\mathrm{P}} - \psi_{\mathrm{P}}^{(opt)} (\eta_Z I_{\mathrm{C}} - Q_Z^{(\mathrm{C})})$	0

A2.3.2 Microzooplankton

The microzooplankton respiration term is defined the same as the mesozooplankton respiration term and is shown in Equation (A59).

The release of dissolved organic carbon is defined as

$$\left.\frac{\partial Z_{\mathrm{C}}^{(i)}}{\partial t}\right|_{R_{\mathrm{C}}^{(6)}}^{\mathrm{rel}} = \varepsilon_{\mathrm{C}} \left\{ I_{\mathrm{C}} \left(1-\eta_Z\right) \beta_Z + Z_{\mathrm{C}}^{(i)} \left[\left(1 - f_Z^{(O)}\right) d_Z^{(\mathrm{O})} + d_Z \right] \right\} \tag{A67}$$

https://doi.org/10.5194/egusphere-2025-2901
Preprint. Discussion started: 5 August 2025

Table A9. Symbols, values, units, and descriptions for mesozooplankton parameters in the BFM.

Symbol	$Z^{(3)}$	$Z^{(4)}$	Units	Description
$r_Z^{(0)}$	2.0	2.0	d^{-1}	Potential specific growth rate
ν_Z	2.5×10^{-3}	0.025	m^3 (mg C)$^{-1}$ d^{-1}	Specific search volume
b_Z	0.01	0.02	d^{-1}	Basal specific respiration rate
η_Z	0.6	0.6	-	Assimilation efficiency
β_Z	0.3	0.35	-	Excreted fraction of uptake
$\psi_{\mathrm{N}}^{(opt)}$	0.015	0.015	mmol N (mg C)$^{-1}$	Optimal nitrogen quota
$\psi_{\mathrm{P}}^{(opt)}$	1.67×10^{-3}	1.67×10^{-3}	mmol P (mg C)$^{-1}$	Optimal phosphorus quota
d_Z	0.02	0.02	d^{-1}	Specific mortality rate
$d_Z^{(dns)}$	0.01	0.01	m^3 (mg C)$^{-1}$ d^{-1}	Density-dependent specific mortality rate
γ_Z	2.0	2.0	-	Exponent for density-dependent mortality
$h_Z^{(O)}$	30.0	30.0	mmol O_2 m^{-3}	Half saturation value for oxygen

where ε_{C} is the partition between dissolved and particulate excretion of carbon, I_{C} is the total ingestion rate of carbon η_Z is the assimilation efficiency, β_Z is the excreted fraction of uptake, $f_Z^{(O)}$ is the oxygen-dependent regulation factor (Equation (A68)), $d_Z^{(O)}$ is the oxygen-dependent specific mortality rate, and d_Z is the specific mortality rate. The oxygen-dependent regulation factor is defined as

$$f_Z^{(O)} = \frac{O^{(2)}}{O^{(2)} + h_Z^{(O)}} \tag{A68}$$

where $h_Z^{(O)}$ is the half saturation value for oxygen.

The dissolved organic nitrogen and phosphorus release terms are defined as

$$\left.\frac{\partial Z_{\mathrm{j}}^{(i)}}{\partial t}\right|_{R_{\mathrm{j}}^{(1)}}^{\mathrm{rel}} = \varepsilon_j \left\{ I_j \beta_Z Z_{\mathrm{j}}^{(i)} \left[\left(1 - \eta_Z\right) d_Z^{(\mathrm{O})} + d_Z \right] \right\}, \quad j = \mathrm{N}, \mathrm{P} \tag{A69}$$

where ε_j is the partition between dissolved and particulate of either nitrogen or phosphorus and I_j is the total ingestion rate for either nitrogen or phosphorus.

The release of particulate organic carbon, nitrogen, and phosphorus are defined as

$$\left.\frac{\partial Z_{\mathrm{j}}^{(i)}}{\partial t}\right|_{R_{\mathrm{j}}^{(6)}}^{\mathrm{rel}} = \left(1 - \varepsilon_{\mathrm{C}}\right) \left\{ I_{\mathrm{C}} \left(1 - \eta_Z\right) \beta_Z + Z_{\mathrm{C}}^{(i)} \left[\left(1 - f_Z^{(O)}\right) d_Z^{(\mathrm{O})} + d_Z \right] \right\} \tag{A70}$$

$$\left.\frac{\partial Z_{\mathrm{j}}^{(i)}}{\partial t}\right|_{R_{\mathrm{j}}^{(6)}}^{\mathrm{rel}} = \left(1 - \varepsilon_j\right) \left\{ I_j \beta_Z Z_{\mathrm{j}}^{(i)} \left[\left(1 - \eta_Z\right) d_Z^{(\mathrm{O})} + d_Z \right] \right\}, \quad j = \mathrm{N}, \mathrm{P} \tag{A71}$$

https://doi.org/10.5194/egusphere-2025-2901
Preprint. Discussion started: 5 August 2025

The release of ammonium and phosphate are defined as

$$\left.\frac{\partial Z_{\mathrm{N}}^{(i)}}{\partial t}\right|_{N^{(4)}}^{\mathrm{rel}} = \max\left\{0,\ \frac{I_{\mathrm{N}}\left(1-\beta_Z\right)+b_Z f_Z^{(T)} Z_{\mathrm{N}}^{(i)}}{I_{\mathrm{C}}\eta_Z} - \psi_{\mathrm{N}}^{(\mathrm{opt})}\right\} I_{\mathrm{C}}\eta_Z \tag{A72}$$

$$\left.\frac{\partial Z_{\mathrm{P}}^{(i)}}{\partial t}\right|_{N^{(1)}}^{\mathrm{rel}} = \max\left\{0,\ \frac{I_{\mathrm{P}}\left(1-\beta_Z\right)+b_Z f_Z^{(T)} Z_{\mathrm{P}}^{(i)}}{I_{\mathrm{C}}\eta_Z} - \psi_{\mathrm{P}}^{(\mathrm{opt})}\right\} I_{\mathrm{C}}\eta_Z \tag{A73}$$

where $\psi_{\mathrm{N}}^{(\mathrm{opt})}$ and $\psi_{\mathrm{P}}^{(\mathrm{opt})}$ are the optimal nitrogen and phosphorus quotas, respectively.

Table A10. Symbols, values, units, and descriptions for microzooplankton parameters in the BFM.

Symbol	$Z^{(5)}$	$Z^{(6)}$	Units	Description
$r_Z^{(0)}$	2.0	5.0	d^{-1}	Potential specific growth rate
μ_Z	50.0	50.0	$\mathrm{m}^3\ (\mathrm{mg\ C})^{-1}\ \mathrm{d}^{-1}$	Half saturation food concentration for preference factor
b_Z	0.02	0.02	d^{-1}	Basal specific respiration rate
η_Z	0.5	0.3	-	Assimilation efficiency
β_Z	0.25	0.35	-	Excreted fraction of uptake
$\psi_{\mathrm{N}}^{(opt)}$	1.28×10^{-2}	1.28×10^{-2}	$\mathrm{mmol\ N\ (mg\ C)}^{-1}$	Optimal nitrogen quota
$\psi_{\mathrm{P}}^{(opt)}$	1.85×10^{-3}	1.85×10^{-3}	$\mathrm{mmol\ P\ (mg\ C)}^{-1}$	Optimal phosphorus quota
d_Z	1.0×10^{-6}	1.0×10^{-6}	d^{-1}	Specific mortality rate
$d_Z^{(O)}$	0.25	0.25	$\mathrm{m}^3\ (\mathrm{mg\ C})^{-1}\ \mathrm{d}^{-1}$	Oxygen-dependent specific mortality rate
$h_Z^{(O)}$	0.5	0.5	$\mathrm{mmol\ O_2\ m}^{-3}$	Half saturation value for oxygen

A3 Non-living Organic Components

The non-living organic components include dissolved organic matter and particulate organic matter.

A3.1 Dissolved Organic Matter

Dissolved organic matter (DOM) is part of the non-living organic CFF and the BFM has carbon, nitrogen, and phosphorus constituents of DOM. The rate equations for each DOM species are

$$\left.\frac{\partial R_{\mathrm{C}}^{(1)}}{\partial t}\right|_{\mathrm{bio}} = \sum_{j=1}^{4}\left.\frac{\partial P_{\mathrm{C}}^{(j)}}{\partial t}\right|_{R_{\mathrm{C}}^{(1)}}^{\mathrm{lys}} + \left.\frac{\partial B_{\mathrm{C}}}{\partial t}\right|_{R_{\mathrm{C}}^{(1)}}^{\mathrm{lys}} - \left.\frac{\partial B_{\mathrm{C}}}{\partial t}\right|_{R_{\mathrm{C}}^{(1)}}^{\mathrm{upt}} + \sum_{k=5,6}\left.\frac{\partial Z_{\mathrm{C}}^{(k)}}{\partial t}\right|_{R_{\mathrm{C}}^{(1)}}^{\mathrm{rel}} \tag{A74}$$

$$\left.\frac{\partial R_{\mathrm{N}}^{(1)}}{\partial t}\right|_{\mathrm{bio}} = \sum_{j=1}^{4}\left.\frac{\partial P_{\mathrm{N}}^{(j)}}{\partial t}\right|_{R_{\mathrm{N}}^{(1)}}^{\mathrm{lys}} + \sum_{j=1}^{4}\min\left[0,\ \left.\frac{\partial P_{\mathrm{N}}^{(j)}}{\partial t}\right|_{R_{\mathrm{N}}^{(3)}}^{\mathrm{upt}} + \left.\frac{\partial P_{\mathrm{N}}^{(j)}}{\partial t}\right|_{R_{\mathrm{N}}^{(4)}}^{\mathrm{upt}}\right] - \left.\frac{\partial B_{\mathrm{C}}}{\partial t}\right|_{R_{\mathrm{N}}^{(1)}}^{\mathrm{lys}} - \frac{R_{\mathrm{N}}^{(1)}}{R_{\mathrm{C}}^{(1)}}\left.\frac{\partial B_{\mathrm{C}}}{\partial t}\right|_{R_{\mathrm{C}}^{(1)}}^{\mathrm{upt}} + \sum_{k=5,6}\left.\frac{\partial Z_{\mathrm{N}}^{(k)}}{\partial t}\right|_{R_{\mathrm{N}}^{(1)}}^{\mathrm{rel}} \tag{A75}$$

https://doi.org/10.5194/egusphere-2025-2901
Preprint. Discussion started: 5 August 2025

$$\left.\frac{\partial R_{\mathrm{P}}^{(1)}}{\partial t}\right|_{\mathrm{bio}} = \sum_{j=1}^{4} \left.\frac{\partial P_{\mathrm{P}}^{(j)}}{\partial t}\right|_{R_{\mathrm{P}}^{(1)}}^{\mathrm{lys}} + \sum_{j=1}^{4} \min\left[0, \left.\frac{\partial P_{\mathrm{P}}^{(j)}}{\partial t}\right|_{R_{\mathrm{N}}^{(1)}}^{\mathrm{upt}}\right] - \left.\frac{\partial B_{\mathrm{C}}}{\partial t}\right|_{R_{\mathrm{P}}^{(1)}}^{\mathrm{lys}} - \left.\frac{R_{\mathrm{P}}^{(1)}}{R_{\mathrm{C}}^{(1)}}\frac{\partial B_{\mathrm{C}}}{\partial t}\right|_{R_{\mathrm{C}}^{(1)}}^{\mathrm{upt}} + \sum_{k=5,6} \left.\frac{\partial Z_{\mathrm{P}}^{(k)}}{\partial t}\right|_{R_{\mathrm{P}}^{(1)}}^{\mathrm{rel}} \tag{A76}$$

$$\left.\frac{\partial R_{\mathrm{C}}^{(2)}}{\partial t}\right|_{\mathrm{bio}} = \sum_{j=1}^{4} \left.\frac{\partial P_{\mathrm{C}}^{(j)}}{\partial t}\right|_{R_{\mathrm{C}}^{(2)}}^{\mathrm{lys}} - \left.\frac{\partial B_{\mathrm{C}}}{\partial t}\right|_{R_{\mathrm{C}}^{(2)}}^{\mathrm{upt}} + \left.\frac{\partial B_{\mathrm{C}}}{\partial t}\right|_{R_{\mathrm{C}}^{(2)}}^{\mathrm{rel}} \tag{A77}$$

$$\left.\frac{\partial R_{\mathrm{C}}^{(3)}}{\partial t}\right|_{\mathrm{bio}} = -\left.\frac{\partial B_{\mathrm{C}}}{\partial t}\right|_{R_{\mathrm{C}}^{(3)}}^{\mathrm{upt}} + \left.\frac{\partial B_{\mathrm{C}}}{\partial t}\right|_{R_{\mathrm{C}}^{(3)}}^{\mathrm{rel}} \tag{A78}$$

The source and sink terms for the DOM rate equations have been defined previously in Section A2.3.

A3.2 Particulate Organic Matter

Particulate organic matter (POM) is part of the non-living organic CFF and the BFM has carbon, nitrogen, and phosphorus constituents of POM. The rate equations for each POM constituent are

$$\left.\frac{\partial R_{\mathrm{C}}^{(6)}}{\partial t}\right|_{\mathrm{bio}} = \sum_{j=1}^{4} \left.\frac{\partial P_{\mathrm{C}}^{(j)}}{\partial t}\right|_{R_{\mathrm{C}}^{(6)}}^{\mathrm{lys}} + \left.\frac{\partial B_{\mathrm{C}}}{\partial t}\right|_{R_{\mathrm{C}}^{(6)}}^{\mathrm{lys}} - \left.\frac{\partial B_{\mathrm{C}}}{\partial t}\right|_{R_{\mathrm{C}}^{(1)}}^{\mathrm{upt}} + \sum_{k=3}^{6} \left.\frac{\partial Z_{\mathrm{C}}^{(k)}}{\partial t}\right|_{R_{\mathrm{C}}^{(6)}}^{\mathrm{rel}} \tag{A79}$$

$$\left.\frac{\partial R_{\mathrm{N}}^{(6)}}{\partial t}\right|_{\mathrm{bio}} = \sum_{j=1}^{4} \left.\frac{\partial P_{\mathrm{N}}^{(j)}}{\partial t}\right|_{R_{\mathrm{N}}^{(6)}}^{\mathrm{lys}} + \sum_{j=1}^{4} \min\left[0, \left.\frac{\partial P_{\mathrm{N}}^{(j)}}{\partial t}\right|_{R_{\mathrm{N}}^{(3)}}^{\mathrm{upt}} + \left.\frac{\partial P_{\mathrm{N}}^{(j)}}{\partial t}\right|_{R_{\mathrm{N}}^{(4)}}^{\mathrm{upt}}\right] - \left.\frac{\partial B_{\mathrm{C}}}{\partial t}\right|_{R_{\mathrm{N}}^{(6)}}^{\mathrm{lys}} - \left.\frac{R_{\mathrm{N}}^{(6)}}{R_{\mathrm{C}}^{(6)}}\frac{\partial B_{\mathrm{C}}}{\partial t}\right|_{R_{\mathrm{C}}^{(1)}}^{\mathrm{upt}} + \sum_{k=3}^{6} \left.\frac{\partial Z_{\mathrm{N}}^{(k)}}{\partial t}\right|_{R_{\mathrm{N}}^{(6)}}^{\mathrm{rel}} \tag{A80}$$

$$\left.\frac{\partial R_{\mathrm{P}}^{(6)}}{\partial t}\right|_{\mathrm{bio}} = \sum_{j=1}^{4} \left.\frac{\partial P_{\mathrm{P}}^{(j)}}{\partial t}\right|_{R_{\mathrm{P}}^{(6)}}^{\mathrm{lys}} + \sum_{j=1}^{4} \min\left[0, \left.\frac{\partial P_{\mathrm{P}}^{(j)}}{\partial t}\right|_{R_{\mathrm{N}}^{(6)}}^{\mathrm{upt}}\right] - \left.\frac{\partial B_{\mathrm{C}}}{\partial t}\right|_{R_{\mathrm{P}}^{(1)}}^{\mathrm{lys}} - \left.\frac{R_{\mathrm{P}}^{(6)}}{R_{\mathrm{C}}^{(6)}}\frac{\partial B_{\mathrm{C}}}{\partial t}\right|_{R_{\mathrm{C}}^{(6)}}^{\mathrm{upt}} + \sum_{k=3}^{6} \left.\frac{\partial Z_{\mathrm{P}}^{(k)}}{\partial t}\right|_{R_{\mathrm{P}}^{(6)}}^{\mathrm{rel}} \tag{A81}$$

$$\left.\frac{\partial R_{\mathrm{S}}^{(6)}}{\partial t}\right|_{\mathrm{bio}} = \left.\frac{\partial P_{\mathrm{P}}^{(1)}}{\partial t}\right|_{R_{\mathrm{P}}^{(6)}}^{\mathrm{lys}} + \frac{P_{\mathrm{S}}^{(1)}}{P_{\mathrm{C}}^{(1)}} \sum_{j=3}^{6} \left.\frac{\partial Z_{\mathrm{C}}^{(j)}}{\partial t}\right|_{P_{\mathrm{C}}^{(1)}}^{\mathrm{prd}} - \left.\frac{\partial R_{\mathrm{S}}^{(6)}}{\partial t}\right|_{\mathrm{N}^{(5)}}^{\mathrm{rmn}} \tag{A82}$$

The silicate dissolution term is defined as

$$\left.\frac{\partial R_{\mathrm{S}}^{(6)}}{\partial t}\right|_{\mathrm{N}^{(5)}}^{\mathrm{rmn}} = \Lambda_{\mathrm{S}}^{\mathrm{rmn}} f_{\mathrm{S}}^{(T)} R_{\mathrm{S}}^{(6)} \tag{A83}$$

where $\Lambda_{\mathrm{S}}^{\mathrm{rmn}}$ is the constant specific dissolution rate and $f_{\mathrm{S}}^{(T)}$ is the temperature regulation factor (Equation (A1)). All other source and sink terms for the POM rate equations have been defined previously in Section A2.

https://doi.org/10.5194/egusphere-2025-2901
Preprint. Discussion started: 5 August 2025

A4 Inorganic Components

The inorganic components include dissolved gases, dissolved inorganic nutrients, and inorganic state variables.

A4.1 Dissolved Gases

The rate equations for dissolved oxygen and dissolved carbon dioxide are

$$\left.\frac{\partial O^{(2)}}{\partial t}\right|_{\text{bio}} = \Omega_{\text{C}}^{(O)} \sum_{j=1}^{4} \left(\left.\frac{\partial P_{\text{C}}^{(j)}}{\partial t}\right|_{O^{(3)}}^{\text{gpp}} - \left.\frac{\partial P_{\text{C}}^{(j)}}{\partial t}\right|_{O^{(3)}}^{\text{rsp}} \right) - \Omega_{\text{C}}^{(O)} f_B^{(O)} \left.\frac{\partial B_{\text{C}}}{\partial t}\right|_{O^{(3)}}^{\text{rsp}} - \Omega_{\text{C}}^{(O)} \sum_{k=3}^{6} \left.\frac{\partial Z_{\text{C}}^{(k)}}{\partial t}\right|_{O^{(3)}}^{\text{rsp}} - \Omega_{\text{N}}^{(O)} \left.\frac{\partial N^{(4)}}{\partial t}\right|_{N^{(3)}}^{\text{nit}} - \frac{1}{\Omega_O^{(r)}} \left.\frac{\partial N^{(6)}}{\partial t}\right|^{\text{reox}} + \left.\frac{\partial O^{(2)}}{\partial t}\right|^{\text{wind}} \tag{A84}$$

$$\left.\frac{\partial O^{(3)}}{\partial t}\right|_{\text{bio}} = \sum_{j=1}^{4} \left(\left.\frac{\partial P_{\text{C}}^{(j)}}{\partial t}\right|_{O^{(3)}}^{\text{gpp}} - \left.\frac{\partial P_{\text{C}}^{(j)}}{\partial t}\right|_{O^{(3)}}^{\text{rsp}} \right) + \left.\frac{\partial B_{\text{C}}}{\partial t}\right|_{O^{(3)}}^{\text{rsp}} \sum_{k=3}^{6} \left.\frac{\partial Z_{\text{C}}^{(k)}}{\partial t}\right|_{O^{(3)}}^{\text{rsp}} + \left.\frac{\partial O^{(3)}}{\partial t}\right|^{\text{flux}} \tag{A85}$$

where $\Omega_{\text{C}}^{(O)}$, $\Omega_{\text{N}}^{(O)}$, and $\Omega_O^{(r)}$ are stoichiometric coefficients for carbon, nitrogen, and oxygen, respectively. The nitrification term is defined as

$$\left.\frac{\partial N^{(4)}}{\partial t}\right|_{N^{(3)}}^{\text{nit}} = \Lambda_{\text{N}^{(4)}}^{\text{nit}} f_{\text{N}}^{(T)} \frac{O^{(2)}}{O^{(2)} + h_O} N^{(6)} \tag{A86}$$

where $\Lambda_{\text{N}^{(4)}}^{\text{nit}}$ is the specific nitrification rate, $f_{\text{N}}^{(T)}$ is the temperature regulation factor (Equation (A1)), and h_O is the half saturation oxygen concentration.

The reoxidation rate of reduction equivalents is defined as

$$\left.\frac{\partial N^{(6)}}{\partial t}\right|^{\text{reox}} = \Lambda_{\text{N}^{(6)}}^{\text{reox}} f_{\text{N}}^{(T)} \frac{O^{(2)}}{O^{(2)} + h_O} N^{(6)} \tag{A87}$$

where$\Lambda_{\text{N}^{(6)}}^{\text{reox}}$ is the specific reoxidation rate.

The oxygen aeration of the surface layer by wind, $\left.\frac{dO^{(2)}}{dt}\right|^{\text{wind}}$, is calculated using the description provided by Weiss (1970) and the flux of dissolved inorganic carbon, $\left.\frac{dO^{(3)}}{dt}\right|^{\text{flux}}$, is based on Wanninkhof (1992)'s description. All other source and sink terms for the dissolved gases have been defined previously in Section A2.

A4.2 Dissolved Inorganic Nutrients

The inorganic nutrients include phosphate, nitrate, ammonium, and silicate. The rate equations for each of the inorganic nutrients are

$$\left.\frac{\partial N^{(1)}}{\partial t}\right|_{\text{bio}} = -\sum_{j=1}^{4} \left.\frac{\partial P_{\text{P}}^{(j)}}{\partial t}\right|_{N^{(1)}}^{\text{upt}} + \left.\frac{\partial B_{\text{P}}}{\partial t}\right|_{N^{(1)}}^{\text{upt, rel}} + \sum_{k=3}^{6} \left.\frac{\partial Z_{\text{P}}^{(k)}}{\partial t}\right|_{N^{(1)}}^{\text{rel}} \tag{A88}$$

https://doi.org/10.5194/egusphere-2025-2901
Preprint. Discussion started: 5 August 2025

$$\left.\frac{\partial N^{(3)}}{\partial t}\right|_{\text{bio}} = -\sum_{j=1}^{4} \left.\frac{\partial P_{\text{N}}^{(j)}}{\partial t}\right|_{N^{(3)}}^{\text{upt}} + \left.\frac{\partial N^{(4)}}{\partial t}\right|_{N^{(3)}}^{\text{nit}} - \left.\frac{\partial N^{(3)}}{\partial t}\right|^{\text{denit}} \tag{A89}$$

$$\left.\frac{\partial N^{(4)}}{\partial t}\right|_{\text{bio}} = -\sum_{j=1}^{4} \left.\frac{\partial P_{\text{N}}^{(j)}}{\partial t}\right|_{N^{(4)}}^{\text{upt}} + \left.\frac{\partial B_{\text{N}}}{\partial t}\right|_{N^{(4)}}^{\text{upt, rel}} + \sum_{k=3}^{6} \left.\frac{\partial Z_{\text{N}}^{(k)}}{\partial t}\right|_{N^{(1)}}^{\text{rel}} - \left.\frac{\partial N^{(4)}}{\partial t}\right|_{N^{(3)}}^{\text{nit}} \tag{A90}$$

$$\left.\frac{\partial N^{(5)}}{\partial t}\right|_{\text{bio}} = -\left.\frac{\partial P_{\text{S}}^{(1)}}{\partial t}\right|_{N^{(5)}}^{\text{upt}} + \left.\frac{\partial R_{\text{S}}^{(6)}}{\partial t}\right|_{\text{N}^{(5)}}^{\text{rmn}} \tag{A91}$$

$$\left.\frac{\partial O^{(4)}}{\partial t}\right|_{\text{bio}} = \left.\frac{\partial N^{(3)}}{\partial t}\right|^{\text{denit}} \tag{A92}$$

The denitrification flux is defined as

$$\left.\frac{\partial N^{(3)}}{\partial t}\right|^{\text{denit}} = \Lambda_{\text{N}^{(3)}}^{\text{denit}} f_{\text{N}}^{(T)} \left[\frac{1}{\mathscr{M}_O} \Omega_{\text{C}}^{(O)} \left(1 - f_B^{(O)}\right) \left.\frac{\partial B_{\text{C}}}{\partial t}\right|_{O^{(3)}}^{\text{rsp}}\right] N^{(3)} \tag{A93}$$

where $\Lambda_{\text{N}^{(3)}}^{\text{denit}}$ is the specific denitrification rate, $f_{\text{N}}^{(T)}$ is the temperature regulation factor (Equation (A1)), $\mathscr{M}_O$ is the reference anoxic mineralization rate, $\Omega_{\text{C}}^{(O)}$ is the stoichiometric coefficient for oxygen reaction, and $f_B^{(O)}$ is the oxygen non-dimensional regulating factor (Equation (A50)). All other source and sink terms for the dissolved inorganic nutrients have been defined previously in Sections A2 and A4.

A4.3 Inorganic Species

The rate equations for total alkalinity and reduction equivalents are

$$\left.\frac{\partial O^{(5)}}{\partial t}\right|_{\text{bio}} = -\left.\frac{\partial N^{(3)}}{\partial t}\right|_{\text{bio}} + \left.\frac{\partial N^{(4)}}{\partial t}\right|_{\text{bio}} \quad \text{if } \texttt{alk\_flag = True}\text{, otherwise} \quad \left.\frac{\partial O^{(5)}}{\partial t}\right|_{\text{bio}} = 0 \tag{A94}$$

$$\left.\frac{\partial N^{(6)}}{\partial t}\right|_{\text{bio}} = \Omega_O^{(r)} \Omega_{\text{C}}^{(O)} \left(1 - f_B^{(O)}\right) \left.\frac{\partial B_{\text{C}}}{\partial t}\right| \Omega_O^{(r)} \tilde{\Omega}_{\text{N}}^{(O)} \left.\frac{\partial N^{(3)}}{\partial t}\right|^{\text{denit}} - \left.\frac{\partial N^{(6)}}{\partial t}\right|^{\text{reox}} \tag{A95}$$

The source and sink terms for the inorganic state variables have been defined previously in Sections A2 and A4. $\Omega_O^{(r)}$, $\Omega_{\text{C}}^{(O)}$, and $\tilde{\Omega}_{\text{N}}^{(O)}$ are the stoichiometric coefficients for oxic-anoxic reaction, oxygen reaction, and denitrification reaction, respectively.

https://doi.org/10.5194/egusphere-2025-2901
Preprint. Discussion started: 5 August 2025

Table A11. Symbols, values, units, and descriptions for the non-living organic CFF and the inorganic CFF parameters within the BFM.

Symbol	Value	Units	Description
Λ_S^{rmn}	0.02	d^{-1}	Specific dissolution rate of biogenic silica
$\Lambda_{R^{(6)}}^{reox}$	0.05	d^{-1}	Specific dissolution rate of reduction equivalents
$\Lambda_{N^{(4)}}^{nit}$	0.01	d^{-1}	Specific nitrification rate
$\Lambda_{N^{(3)}}^{denit}$	0.35	d^{-1}	Specific denitrification rate
h_O	10.0	mmol O_2 m^{-3}	Half saturation oxygen concentration
h_r	1.0	mmol HS^- m^{-3}	Half saturation oxygen concentration for anoxic processes
$\mathscr{M}_O$	1.0	mmol O_2 m^{-3} d^{-1}	Reference anoxic mineralization rate
`alk_flag`	`FALSE`	-	Logical parameter for total alkalinity calculation

B Princeton Ocean Model

POM is a three-dimensional ocean circulation model developed by Blumberg and Mellor (1987). Mellor (2003) adapted this into a one-dimensional solver, POM1D, which includes only the vertical coordinate. Briefly, the diagnostic mode of POM1D, which is used in this study, solves the momentum equations for the horizontal velocity components (U,V) given by

$$\frac{\partial U}{\partial t} - fV = \frac{\partial}{\partial z}\left(K_M \frac{\partial U}{\partial t}\right) \tag{B1}$$

$$\frac{\partial V}{\partial t} - fU = \frac{\partial}{\partial z}\left(K_M \frac{\partial V}{\partial t}\right), \tag{B2}$$

where the Coriolis parameter, f, is described by the angular velocity of the Earth, Ω, and latitude, ϕ, as

$$f = 2\Omega \sin\phi\,. \tag{B3}$$

The vertical viscosity and diffusivity coefficients, K_M and K_H respectively, are calculated using Mellor and Yamada's closure hypothesis as

$$K_M = qlS_M \tag{B4}$$

$$K_H = qlS_H\,, \tag{B5}$$

where q is the turbulent velocity, l is the length scale, and S_M and S_H are empirical functions. The turbulent kinetic energy and length scale are obtained by solving

$$\frac{\partial}{\partial t}\left(\frac{q^2}{2}\right) = \frac{\partial}{\partial z}\left[K_q \frac{\partial}{\partial z}\left(\frac{q^2}{2}\right)\right] + \left[\left(\frac{\partial U}{\partial z}\right)^2 + \left(\frac{\partial V}{\partial z}\right)^2\right] + \frac{g}{\rho_0} K_H \frac{\partial \rho}{\partial z} - \frac{q^3}{B_1 l} \tag{B6}$$

https://doi.org/10.5194/egusphere-2025-2901
Preprint. Discussion started: 5 August 2025

$$\frac{\partial}{\partial t}(q^2 l) = \frac{\partial}{\partial z}\left[K_q \frac{\partial}{\partial z}(q^2 l)\right] + E_1 l K_M \left[\left(\frac{\partial U}{\partial z}\right)^2 + \left(\frac{\partial V}{\partial z}\right)^2\right] + E_1 l \frac{g}{\rho_0} K_H \frac{\partial \rho}{\partial z} - \frac{q^3}{B_1}\tilde{W}\,, \tag{B7}$$

where $g = 9.81m\ s^{-1}$, $\rho_0 = 1025kg\ m^{-3}$, $K_q = \kappa K_H$ is the vertical diffusivity for turbulence, $\kappa = 0.4$ is the von Karman constant, $\tilde{W}$ is a function of the distance between rigid boundaries, and B_1 and E_1 are empirical constants.

Boundary conditions are necessary for solving the momentum (B1 and B2) and turbulence (B6 and B7) equations. The boundary conditions for horizontal velocity components are

$$K_M \frac{\partial U}{\partial z}\bigg|_{z=0} = \tau_w^{(x)} \tag{B8}$$

$$K_M \frac{\partial V}{\partial z}\bigg|_{z=0} = \tau_w^{(y)} \tag{B9}$$

$$K_M \frac{\partial \vec{U}}{\partial z}\bigg|_{z=-H} = \vec{\tau}_b\,. \tag{B10}$$

The wind stress, $\vec{\tau}_w$, and bottom drag coefficient, $\vec{\tau}_b$, are described by

$$\vec{\tau}_w = (\tau_w^{(x)}, \tau_w^{(y)}) \tag{B11}$$

$$\vec{\tau}_b = C_b \left|\vec{U}_b\right| \vec{U}_b\,, \tag{B12}$$

where C_b is the bottom drag coefficient and $\vec{U}_b = (U_b, V_b)$ is the bottom velocity. The boundary conditions for the turbulent kinetic energy are

$$q^2\Big|_{z=0} = B_1^{\frac{2}{3}} \frac{|\vec{\tau}_w|}{C_d} \tag{B13}$$

$$q^2\Big|_{z=-H} = B_1^{\frac{2}{3}} \frac{|\vec{\tau}_b|}{C_b}\,. \tag{B14}$$

Blumberg and Mellor (1987) and Mellor (2003) give full descriptions of the three-dimensional POM and the one-dimensional version (POM1D), respectively.

https://doi.org/10.5194/egusphere-2025-2901
Preprint. Discussion started: 5 August 2025

C Coupled Physical-Biogeochemical Models

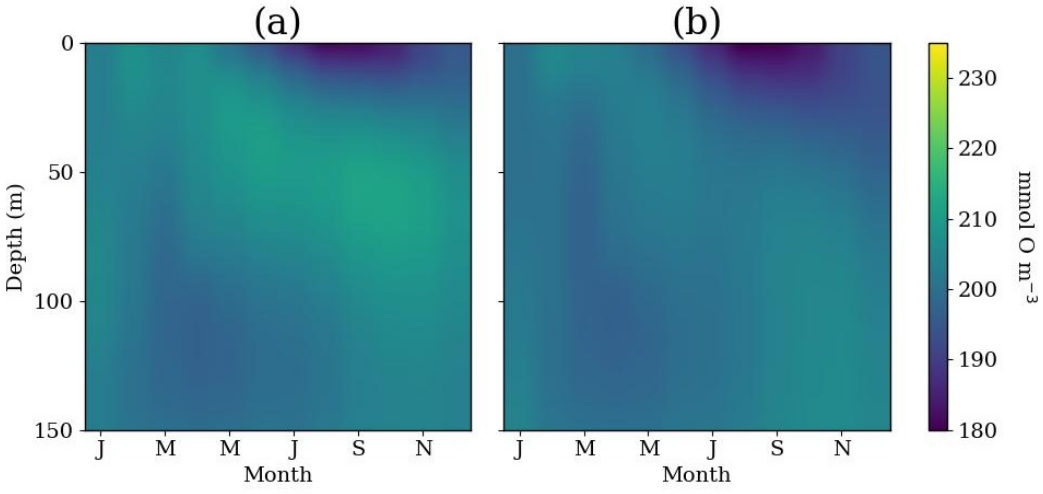

Figure C1. Comparison of (a) pyPOM1D-BFM50 simulation results to (b) pyPOM1D-Oxygen for oxygen concentration (mmol O/m^3). Simulation plots are monthly averages for the second year in the simulation.

https://doi.org/10.5194/egusphere-2025-2901
Preprint. Discussion started: 5 August 2025

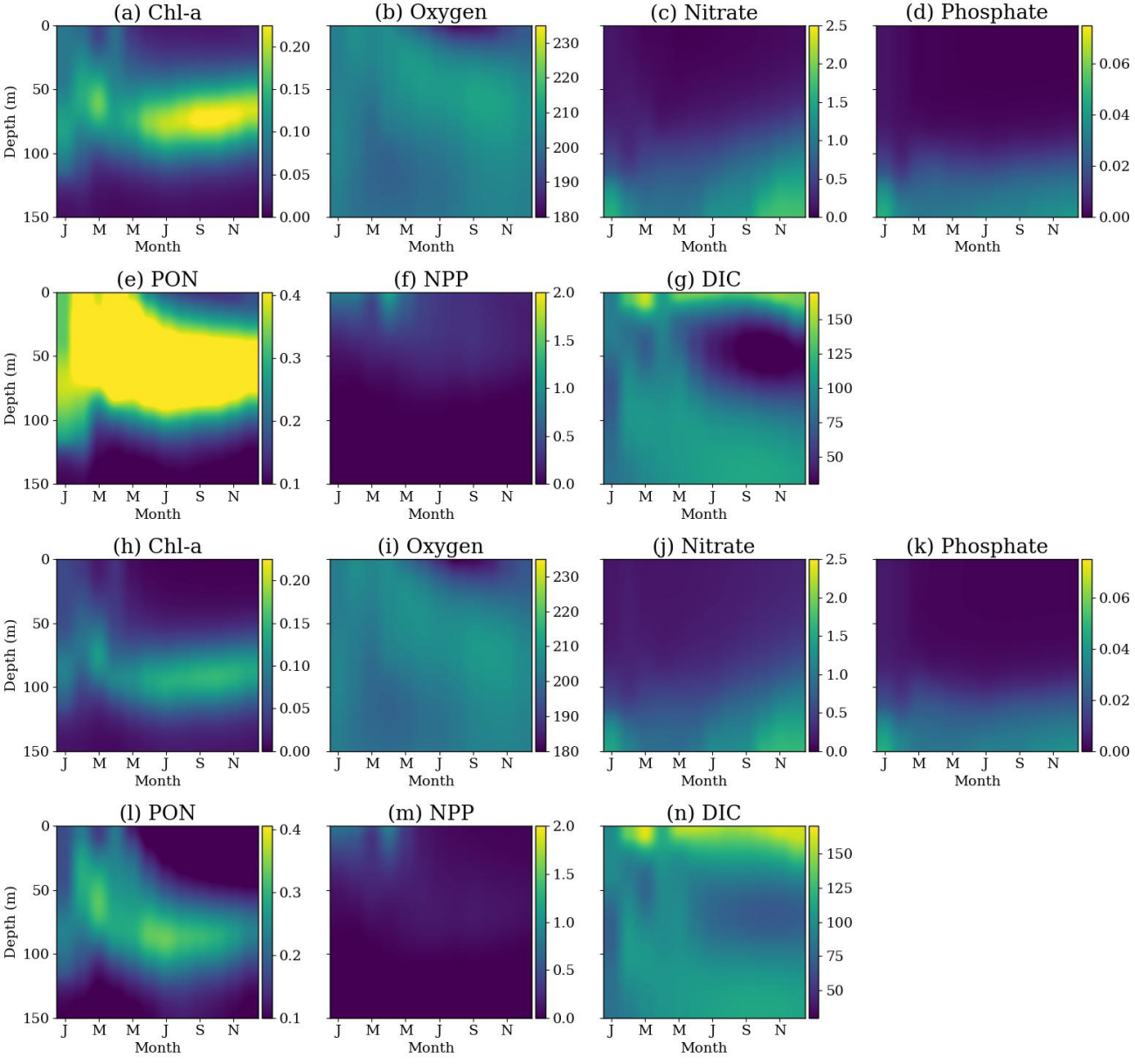

Figure C2. Comparison of pyPOM1D-BFM50 simulation results (rows 1 and 2) to pyPOM1D-BFM23 (rows 3 and 4) for (a,h) chlorophyll-a (mg Chl-a/m^3), (b,i) oxygen (mmol O/m^3), (c,j) nitrate (mmol N/m^3), (d,k) phosphate (mmol P/m^3), (e,l) PON (mg N/m^3), (f,m) NPP (mg C/m^3/day), (g,n) DIC (mg C/m^3). Simulation plots are monthly averages for the second year in the simulation.

https://doi.org/10.5194/egusphere-2025-2901
Preprint. Discussion started: 5 August 2025

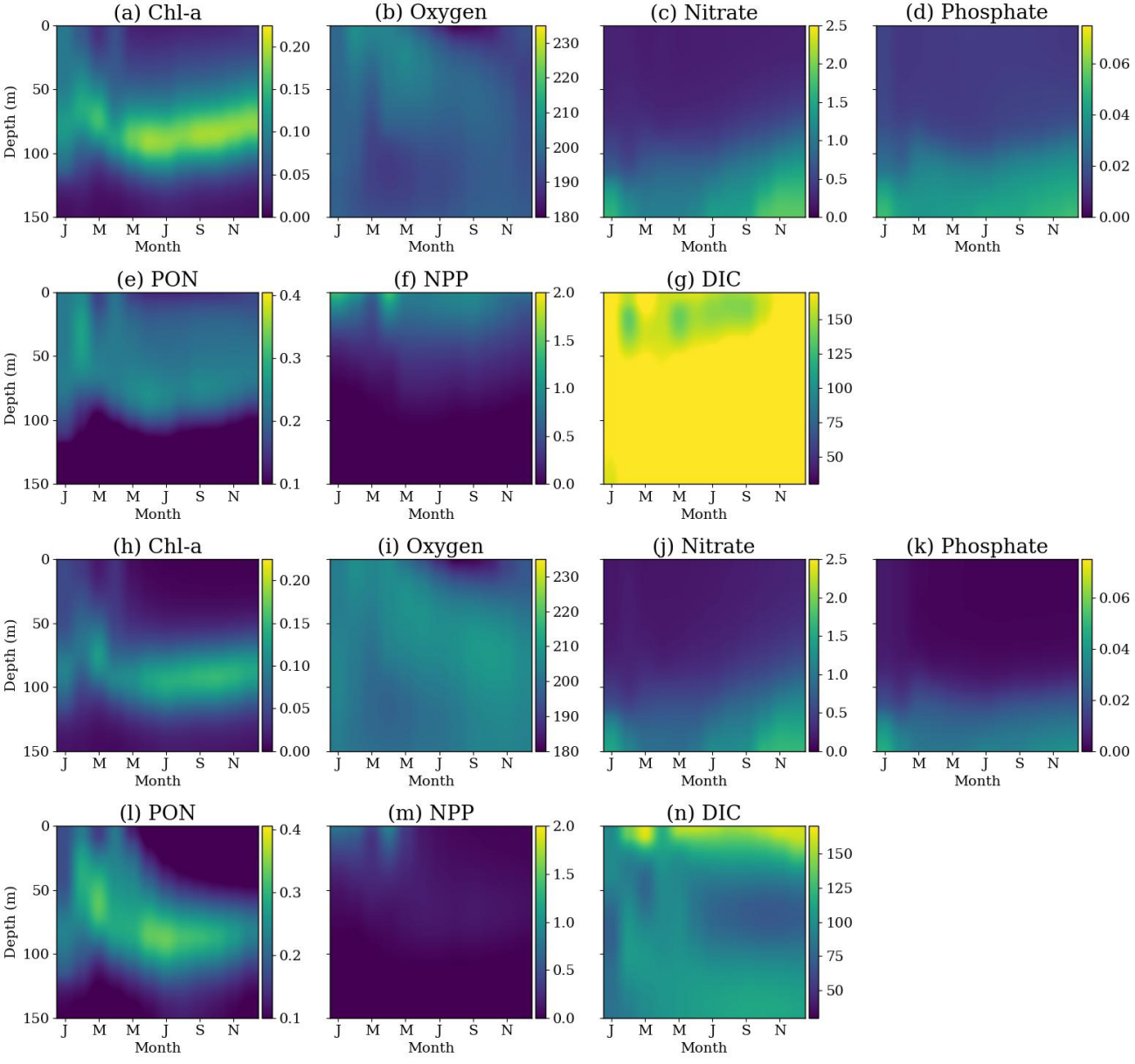

Figure C3. Comparison of BFM17-POM1D simulation results (rows 1 and 2) to pyPOM1D-BFM23 (rows 3 and 4) for (a,h) chlorophyll-a (mg Chl-a/m^3), (b,i) oxygen (mmol O/m^3), (c,j) nitrate (mmol N/m^3), (d,k) phosphate (mmol P/m^3), (e,l) PON (mg N/m^3), (f,m) NPP (mg C/m^3/day), (g,n) DIC (mg C/m^3). Simulation plots are monthly averages for the second year in the simulation.

https://doi.org/10.5194/egusphere-2025-2901
Preprint. Discussion started: 5 August 2025

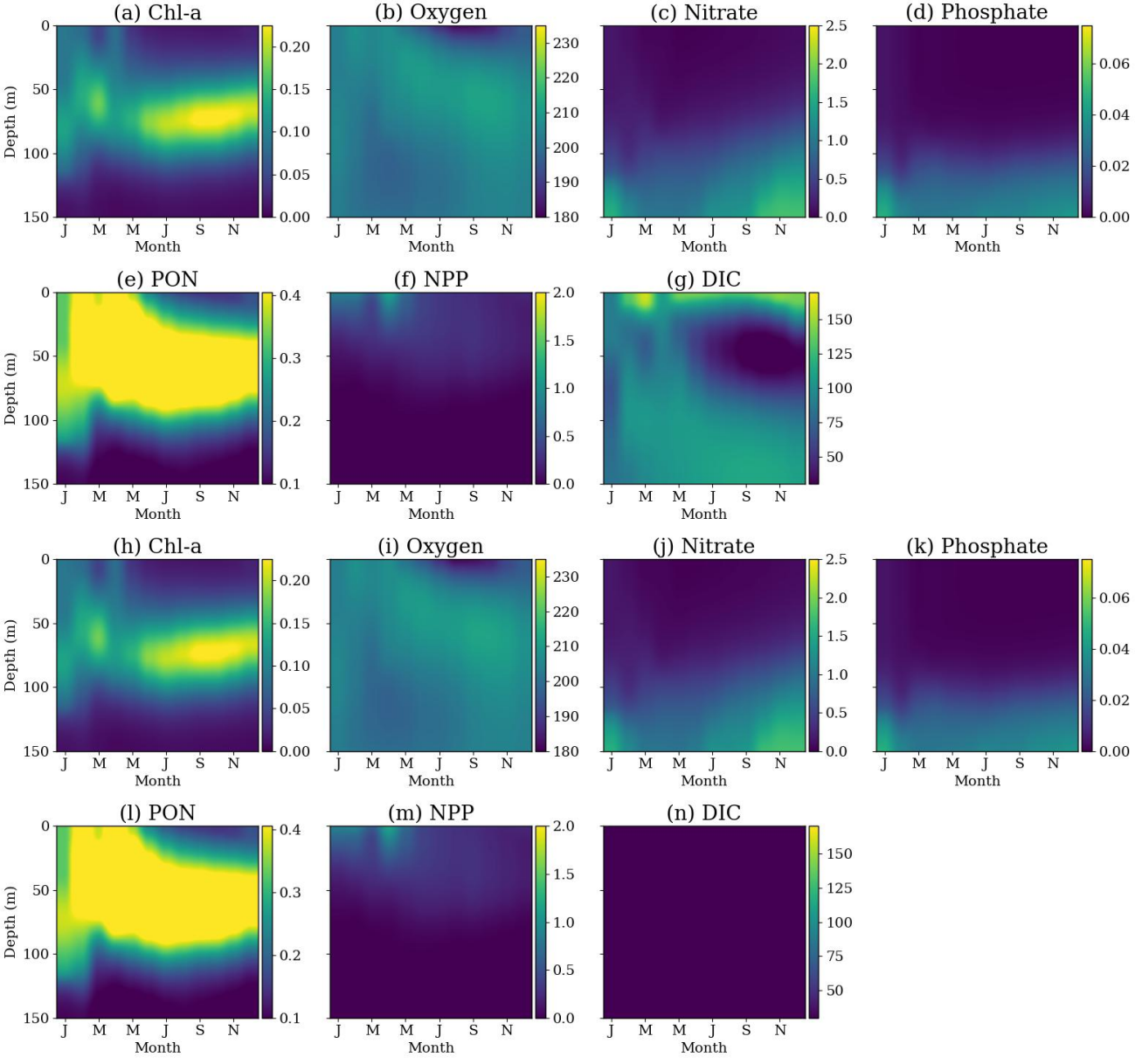

Figure C4. Comparison of pyPOM1D-BFM50 simulation results (rows 1 and 2) to pyPOM1D-BFM34 (rows 3 and 4) for (a,h) chlorophyll-a (mg Chl-a/m^3), (b,i) oxygen (mmol O/m^3), (c,j) nitrate (mmol N/m^3), (d,k) phosphate (mmol P/m^3), (e,l) PON (mg N/m^3), (f,m) NPP (mg C/m^3/day), (g,n) DIC (mg C/m^3). Simulation plots are monthly averages for the second year in the simulation.

https://doi.org/10.5194/egusphere-2025-2901
Preprint. Discussion started: 5 August 2025

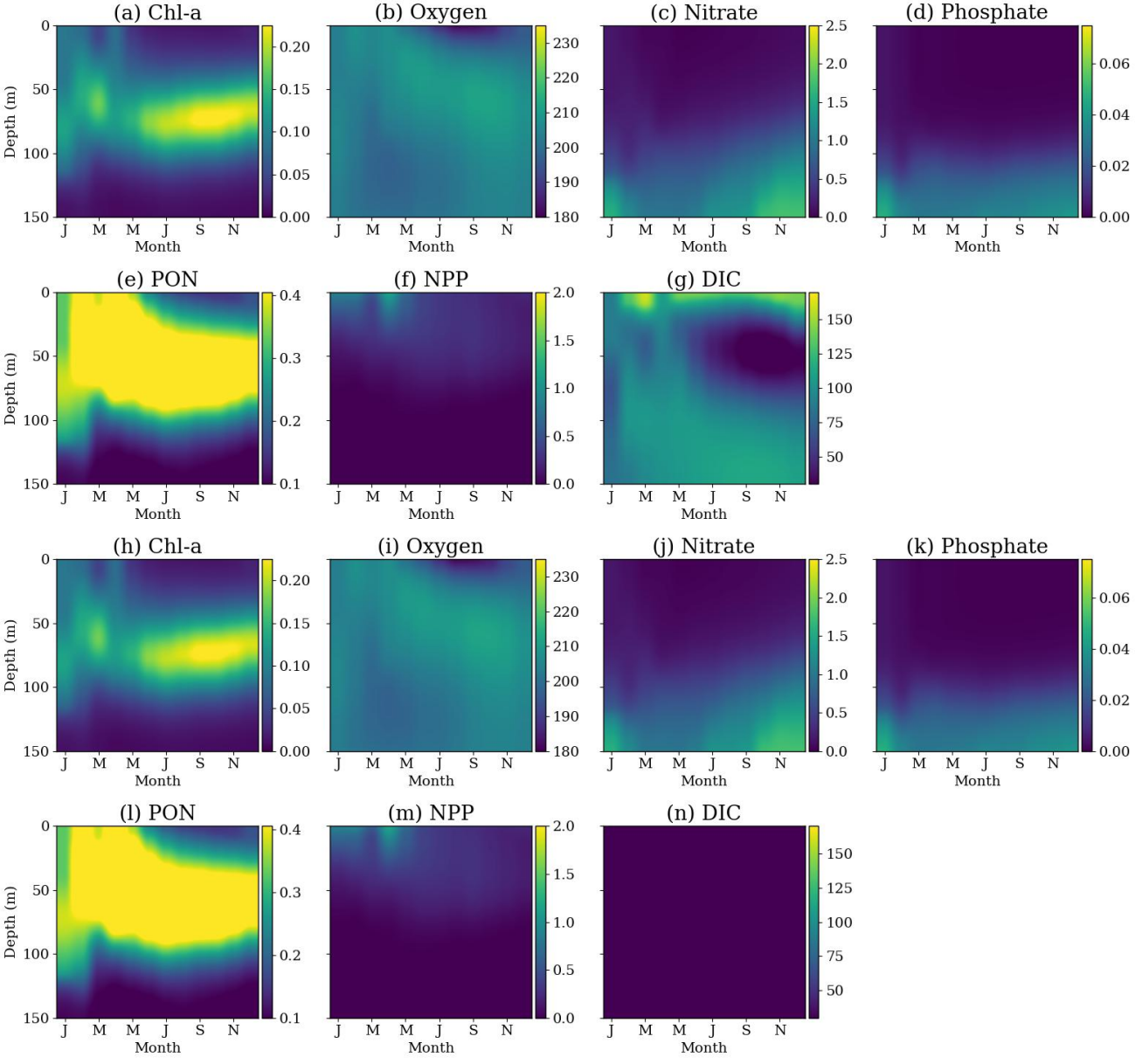

Figure C5. Comparison of pyPOM1D-BFM50 simulation results (rows 1 and 2) to pyPOM1D-BFM35 (rows 3 and 4) for (a,h) chlorophyll-a (mg Chl-a/m^3), (b,i) oxygen (mmol O/m^3), (c,j) nitrate (mmol N/m^3), (d,k) phosphate (mmol P/m^3), (e,l) PON (mg N/m^3), (f,m) NPP (mg C/m^3/day), (g,n) DIC (mg C/m^3). Simulation plots are monthly averages for the second year in the simulation.

https://doi.org/10.5194/egusphere-2025-2901
Preprint. Discussion started: 5 August 2025

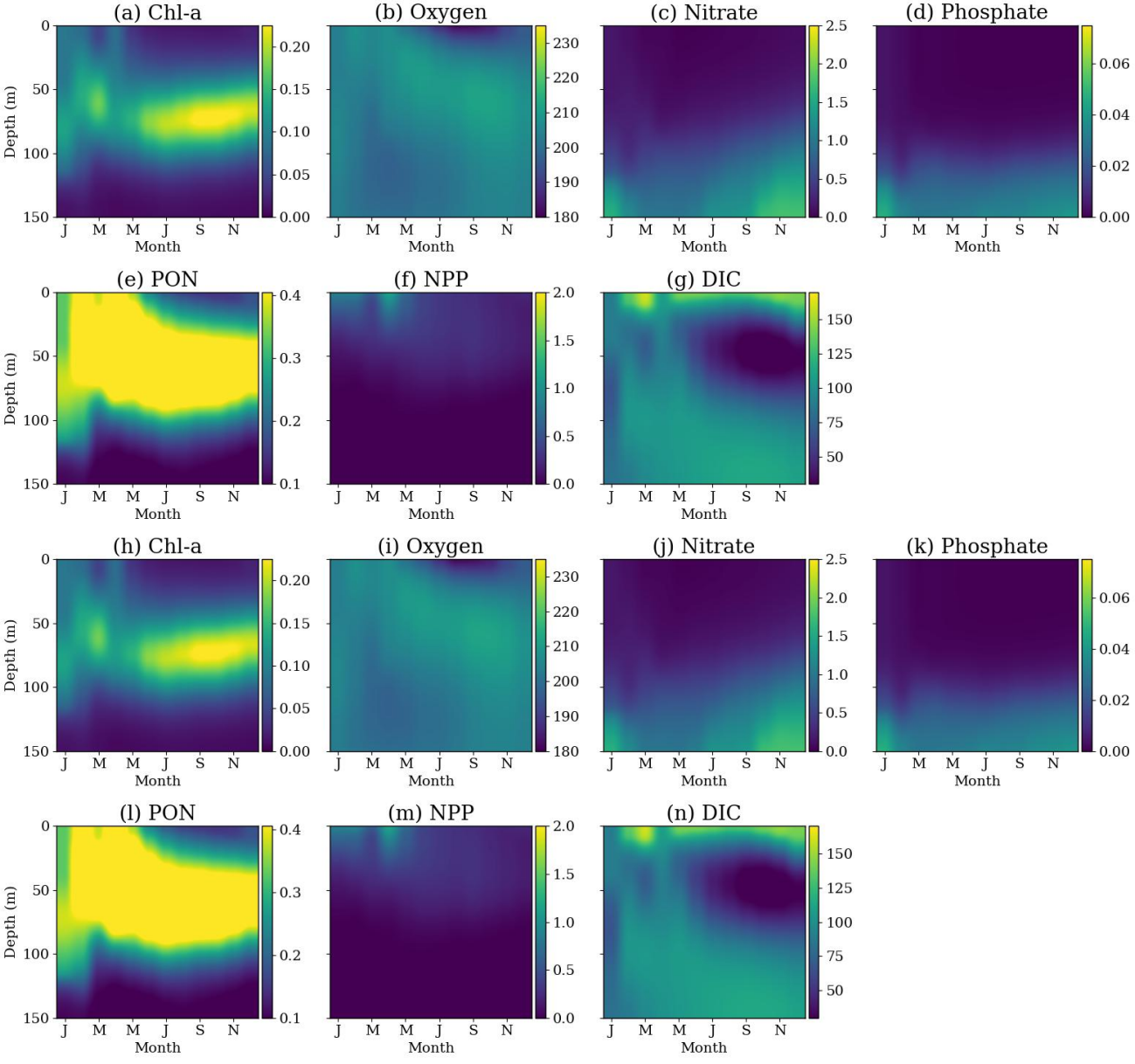

Figure C6. Comparison of pyPOM1D-BFM50 simulation results (rows 1 and 2) to pyPOM1D-BFM36 (rows 3 and 4) for (a,h) chlorophyll-a (mg Chl-a/m^3), (b,i) oxygen (mmol O/m^3), (c,j) nitrate (mmol N/m^3), (d,k) phosphate (mmol P/m^3), (e,l) PON (mg N/m^3), (f,m) NPP (mg C/m^3/day), (g,n) DIC (mg C/m^3). Simulation plots are monthly averages for the second year in the simulation.

https://doi.org/10.5194/egusphere-2025-2901
Preprint. Discussion started: 5 August 2025

References

Benzi, R. and Nelson, D. R.: Fisher equation with turbulence in one dimension, Physica D: Nonlinear Phenomena, 238, 2003 – 2015, https://doi.org/10.1016/j.physd.2009.07.015, 2009.

Bissett, W., Walsh, J., Dieterle, D., and Carder, K.: Carbon cycling in the upper waters of the Sargasso Sea: I. Numerical simulation of differential carbon and nitrogen fluxes, Deep Sea Research Part I: Oceanographic Research Papers, 46, 205 – 269, https://doi.org/10.1016/S0967-0637(98)00062-4, 1999.

Blumberg, A. F. and Mellor, G. L.: A description of a three-dimensional coastal ocean circulation model, in: Three-Dimensional Coastal Ocean Models, pp. 1–16, American Geophysical Union, https://doi.org/10.1029/co004p0001, 1987.

Denman, K. and Peña, M.: The response of two coupled one-dimensional mixed layer/planktonic ecosystem models to climate change in the NE subarctic Pacific Ocean, Deep Sea Research Part II: Topical Studies in Oceanography, 49, 5739 – 5757, https://doi.org/10.1016/S0967-0645(02)00212-6, north Pacific Biogeochemical Processes, 2002.

Dijkstra, E.: A note on two problems in connexion with graphs, Numerische Mathematik, 1, 269–271, https://doi.org/10.1007/BF01386390, 1959.

Fennel, K., Mattern, J. P., Doney, S. C., Bopp, L., Moore, A. M., Wang, B., and Yu, L.: Ocean biogeochemical modelling, Nature Reviews Methods Primers, 2, https://doi.org/10.1038/s43586-022-00154-2, 2022.

Franks, P.: NPZ Models of Plankton Dynamics: Their Construction, Coupling to Physics, and Application, Journal of Oceanography, 58, 379–387, https://doi.org/10.1023/A:1015874028196, 2002.

Galbraith, E. D., Dunne, J. P., Gnanadesikan, A., Slater, R. D., Sarmiento, J. L., Dufour, C. O., de Souza, G. F., Bianchi, D., Claret, M., Rodgers, K. B., and Marvasti, S. S.: Complex functionality with minimal computation: Promise and pitfalls of reduced-tracer ocean biogeochemistry models, Journal of Advances in Modeling Earth Systems, 7, 2012–2028, https://doi.org/10.1002/2015ms000463, 2015.

Heinle, A. and Slawig, T.: Internal dynamics of NPZD type ecosystem models, Ecological Modelling, 254, 33 – 42, https://doi.org/10.1016/j.ecolmodel.2013.01.012, 2013.

Jordan, M. J., Klee, E. F., Hamlington, P. E., Lovenduski, N. S., and Niemeyer, K. E.: Python Princeton Ocean Model - Reduced Biogeochemical Flux Model (pyPOM1D-reducedBFM), https://doi.org/10.5281/zenodo.16624084, 2025a.

Jordan, M. J., Klee, E. F., Hamlington, P. E., Lovenduski, N. S., and Niemeyer, K. E.: Data, plotting scripts, and figures for "Automatic reduction of ocean biogeochemical models: a case study with BFM (v5.3)", https://doi.org/10.5281/zenodo.16624062, 2025b.

Kern, S., McGuinn, M. E., Smith, K. M., Pinardi, N., Niemeyer, K. E., Lovenduski, N. S., and Hamlington, P. E.: Computationally efficient parameter estimation for high-dimensional ocean biogeochemical models, Geoscientific Model Development Discussions, 2023, 1–34, https://doi.org/10.5194/gmd-2023-107, 2023.

Klee, E.: Modified DRGEP method, https://doi.org/10.5281/zenodo.4021414, 2020a.

Klee, E. F.: Python Biogeochemical Flux Model, https://doi.org/10.5281/zenodo.4021274, 2020b.

Lancelot, C., Spitz, Y., Gypens, N., Ruddick, K., Becquevort, S., Rousseau, V., Lacroix, G., and Billen, G.: Modelling diatom and Phaeocystis blooms and nutrient cycles in the Southern Bight of the North Sea: the MIRO model, Marine Ecology Progress Series, 289, 63–78, https://doi.org/10.3354/meps289063, 2005.

Le Quéré, C., Harrison, S. P., Prentice, I. C., Buitenhuis, E. T., Aumont, O., Bopp, L., Claustre, H., Cotrim Da Cunha, L., Geider, R., Giraud, X., Klaas, C., Kohfeld, K. E., Legendre, L., Manizza, M., Platt, T., Rivkin, R. B., Sathyendranath, S., Uitz, J., Watson, A. J., and Wolf-Gladrow, D.: Ecosystem dynamics based on plankton functional types for global ocean biogeochemistry models, Global Change Biology, 2005.

https://doi.org/10.5194/egusphere-2025-2901
Preprint. Discussion started: 5 August 2025

Lévy, M., Klein, P., and Treguier, A.: Impact of sub-mesoscale physics on production and subduction of phytoplankton in an oligotrophic regime, Journal of Marine Research, 2001.

Lewis, D.: A simple model of plankton population dynamics coupled with a LES of the surface mixed layer, Journal of Theoretical Biology, 234, 565 – 591, https://doi.org/https://doi.org/10.1016/j.jtbi.2004.12.013, 2005.

Lu, T. and Law, C. K.: A directed relation graph method for mechanism reduction, Proceedings of the Combustion Institute, 30, 1333–1341, https://doi.org/10.1016/j.proci.2004.08.145, 2005.

Lu, T. and Law, C. K.: On the applicability of directed relation graphs to the reduction of reaction mechanisms, Combustion and Flame, 146, 472–483, https://doi.org/10.1016/j.combustflame.2006.04.017, 2006a.

Lu, T. and Law, C. K.: Linear time reduction of large kinetic mechanisms with directed relation graph: n-Heptane and iso-octane, Combustion and Flame, 144, 24–36, https://doi.org/10.1016/j.combustflame.2005.02.015, 2006b.

Mellor, G.: Users Guide For A Three-Dimensional, Primitive Equation, Numerical Ocean Model, Atmospheric & Ocean Sciences Program Report, 2003.

Mellor, G. L. and Yamada, T.: Development of a turbulence closure model for geophysical fluid problems, Reviews of Geophysics, 20, 851–875, https://doi.org/https://doi.org/10.1029/RG020i004p00851, 1982.

Moore, J. K., Lindsay, K., Doney, S. C., Long, M. C., and Misumi, K.: Marine Ecosystem Dynamics and Biogeochemical Cycling in the Community Earth System Model [CESM1(BGC)]: Comparison of the 1990s with the 2090s under the RCP4.5 and RCP8.5 Scenarios, Journal of Climate, 26, 9291–9312, https://doi.org/10.1175/JCLI-D-12-00566.1, 2013.

Niemeyer, K. E. and Sung, C.-J.: On the importance of graph search algorithms for DRGEP-based mechanism reduction methods, Combustion and Flame, 158, 1439–1443, https://doi.org/10.1016/j.combustflame.2010.12.010, 2011.

Niemeyer, K. E., Sung, C.-J., and Raju, M. P.: Skeletal Mechanism Generation for Surrogate Fuels Using Directed Relation Graph with Error Propagation and Sensitivity Analysis, Combustion and Flame, 157, 1760–1770, https://doi.org/10.1016/j.combustflame.2009.12.022, 2010.

Pepiot, P. and Pitsch, H.: Systematic Reduction of Large Chemical Mechanisms, 4th Joint Meeting of the U.S. Sections of the Combustion Institute, 2005.

Pepiot-Desjardins, P. and Pitsch, H.: An efficient error-propagation-based reduc- tion method for large chemical kinetic mechanisms, Combustion and Flame, 154, 67–81, https://doi.org/10.1016/j.combustflame.2007.10.020, 2008.

Schartau, M. and Oschlies, A.: Simultaneous data-based optimization of a 1D-ecosystem model at three locations in the North Atlantic: Part I—Method and parameter estimates, Journal of Marine Research, 61, 765–793, https://doi.org/10.1357/002224003322981147, 2003.

Smith, K., Hamlington, P., and Fox-Kemper, B.: Effects of Submesoscale Turbulence on Ocean Tracers, Journal of Geophysical Research: Oceans, 121, https://doi.org/10.1002/2015JC011089, 2015.

Smith, K. M., Hamlington, P. E., Niemeyer, K. E., Fox-Kemper, B., and Lovenduski, N. S.: Effects of Langmuir turbulence on upper ocean carbonate chemistry, Journal of Advances in Modeling Earth Systems, 10, 3030–3048, https://doi.org/10.1029/2018MS001486, 2018.

Smith, K. M., Kern, S., Hamlington, P. E., Zavatarelli, M., Pinardi, N., Klee, E. F., and Niemeyer, K. E.: BFM17 V1.0: Reduced-Order Biogeochemical Flux Model for Upper Ocean Biophysical Simulations, Geoscientific Model Development Discussions, 2020, 1–35, https://doi.org/10.5194/gmd-2020-134, 2020.

Steinberg, D. K., Carlson, C. A., Bates, N. R., Johnson, R. J., Michaels, A. F., and Knap, A. H.: Overview of the US JGOFS Bermuda Atlantic Time-series Study (BATS): a decade-scale look at ocean biology and biogeochemistry, Deep Sea Research Part II: Topical Studies in Oceanography, 48, 1405–1447, https://doi.org/https://doi.org/10.1016/S0967-0645(00)00148-X, 2001.

https://doi.org/10.5194/egusphere-2025-2901
Preprint. Discussion started: 5 August 2025

Stock, C. A., Dunne, J. P., and John, J. G.: Global-scale carbon and energy flows through the marine planktonic food web: An analysis with a coupled physical–biological model, Progress in Oceanography, 120, 1 – 28, https://doi.org/10.1016/j.pocean.2013.07.001, 2014.

Stock, C. A., Dunne, J. P., Fan, S., Ginoux, P., John, J., Krasting, J. P., Laufkötter, C., Paulot, F., and Zadeh, N.: Ocean Biogeochemistry in GFDL's Earth System Model 4.1 and Its Response to Increasing Atmospheric CO_2, Journal of Advances in Modeling Earth Systems, 12, https://doi.org/10.1029/2019ms002043, 2020.

Vichi, M., Masina, S., and Navarra, A.: A generalized model of pelagic biogeochemistry for the global ocean ecosystem. Part II: numerical simulations, jms, 64, 110–134, 2007a.

Vichi, M., Pinardi, N., and Masina, S.: A generalized model of pelagic biogeochemistry for the global ocean ecosystem. Part I: theory, Journal of Marine Systems, 64, 89–109, https://doi.org/10.1016/j.jmarsys.2006.03.006, 2007b.

Vichi, M., Lovato, T., Butenschön, M., Tedesco, L., Lazzari, P., Cossarini, G., Masina, S., Pinardi, N., Solidoro, C., and Zavatarelli, M.: The Biogeochemical Flux Model (BFM): Equation Description and User Manual. BFM version 5.3, BFM Consortium, 2023.

Wanninkhof, R.: Relationship between wind speed and gas exchange over the ocean, Journal of Geophysical Research, 97, 7373–7382, https://doi.org/10.1029/92JC00188, 1992.

Ward, B. A., Schartau, M., Oschlies, A., Martin, A. P., Follows, M. J., and Anderson, T. R.: When is a biogeochemical model too complex? Objective model reduction and selection for North Atlantic time-series sites, Progress in Oceanography, 116, 49–65, https://doi.org/10.1016/j.pocean.2013.06.002, 2013.

Weiss, R.: The solubility of nitrogen, oxygen and argon in water and seawater, Deep Sea Research and Oceanographic Abstracts, 17, 721 – 735, https://doi.org/10.1016/0011-7471(70)90037-9, 1970.

Wiggert, J., Murtugudde, R., and Christian, J.: Annual ecosystem variability in the tropical Indian Ocean: Results of a coupled bio-physical ocean general circulation model, Deep Sea Research Part II: Topical Studies in Oceanography, 2006.